INVESTIGATION OF TRANSITION METAL DICHALCOGENIDE BASED LAYERED SUPERCONDUCTORS

SOUMEN ASH

A thesis submitted for the partial fulfillment of the degree of Doctor of Philosophy

Institute of Nano Science and Technology
Knowledge City, Sector 81, SAS Nagar, Manauli PO, Mohali 140306, Punjab,India.

Indian Institute of Science Education and Research
Knowledge City, Sector 81, SAS Nagar, Manauli PO, Mohali 140306, Punjab,India.

April 2021

Dedicated to my family, friends & teachers
for their endless support and encouragement.

Declaration

The work presented in this thesis has been carried out by me under the guidance of Prof. Ashok K. Ganguli and Prof. Hirendra N. Ghosh at Indian Institute of Technology Delhi, New Delhi and Institute of Nano Science and Technology, Mohali. This work has not been submitted in part or in full for a degree, diploma or a fellowship to any other University or Institute. Whenever contributions of others are involved, every effort has been made to indicate this clearly, with due acknowledgement of collaborative research and discussions. This thesis is a bonafide record of original work done by me and all sources listed within have been detailed in the bibliography.

Place: **Soumen Ash**

Date: **(Candidate)**

In my capacity as the supervisor of the candidate's Ph.D. thesis work, I certify that the above statements by the candidate are true to the best of my knowledge.

Place: **Prof. Ashok K. Ganguli**

Date: **(Supervisor)**

Indian Institute of technology Delhi, New Delhi

Place: **Prof. Hirendra N. Ghosh**

Date: **(Supervisor)**

Institute of Nano Science and Technology, Mohali

Acknowledgements

The pursuit of my research in experimental condensed matter physics for the last few years at IIT Delhi and INST Mohali has finally come to its fulfilment with the completion of my thesis. In this great venture of my Ph.D., I have been benefitted from many creative individuals directly or indirectly. I take this opportunity to convey my token of gratitude to all the people who have made this dissertation possible and because of whom this incredible journey of mine has become the one that I will cherish forever.

First and foremost, I would like to express my utmost gratitude to my supervisor, Prof. Ashok K. Ganguli, for his unparalleled guidance and steadfast support throughout my Ph.D. and for vesting an unfathomed trust in me during trials and tribulations. I am immensely thankful to him and greatly acknowledge all his encouragement, enlightening suggestions, and all the efforts he made to groom me as a researcher. Prof. Ganguli has given me the full privilege of pursuing my scientific ideas and the problems of mutual interest to embark upon, which is an invaluable treasure for a young researcher like me. His proactive nature and the zeal he has towards science are highly motivating and always been a source of inspiration. It is my great honour to have the opportunity to work under his admirable supervision.

I want to record my notes of sincere gratitude to my supervisor, Prof. Hirendra N. Ghosh, for his unwavering support and motivation. I am greatly thankful to him for always being there for me and taking a stand for me in the trying times. His energetic and approachable persona has always helped me to flourish as a young researcher.

In particular, I would like to thank and convey my deepest gratitude to Prof. L. C. Gupta (visiting scientist at Solid State and Nano Materials Lab, Dept. of Chemistry, IIT Delhi and retd. Professor, TIFR Mumbai) for all the exciting scientific discussions we had that always encourage me to perceive a problem scientifically.

He has always been supportive of me and has helped me a lot by sharing his vast knowledge and experience in condensed matter physics. It is my great fortune to have the opportunity to learn from a veteran and knowledgeable person like Prof. Gupta.

I am highly grateful to the Director, INST Mohali, for allowing me to carry out my thesis work at IIT Delhi. At the same time, I want to express my indebtedness to the HoD, Dept. of Chemistry, IIT Delhi, for giving me the opportunity to pursue my research work in the lab at IIT Delhi. I thank Department of Science and Technology (DST), India for providing fellowships through INST Mohali.

I want to express my sincere gratitude to my doctoral committee members for their valuable insights and suggestions. I would like to thank all the faculty members of INST Mohali, IISER Mohali and IIT Delhi. It has always been highly beneficial to have fruitful discussions and exchange scientific ideas with great minds.

The work presented in this thesis is a result of joint collaborative efforts from various research groups across and outside the country. I am very grateful to Prof. S. Patnaik and Mr. Vipin Nagpal (JNU, New Delhi) for carrying out transport measurements on our $PbNbS_2$ and $PbNbSe_2$ samples. I am also very thankful to Prof. A. Sundaresan and Mr. Ravi Shankar P. N. (JNCASR, Bangalore) for performing the magnetic and heat capacity measurements on the $PbNbS_2$ and $PbNbSe_2$ samples and for the transport and magnetic studies of the $SnTaS_2$ system. I would like to acknowledge the primary data we received for some of our early samples from Prof. K. Ramanujachary (Rowan University, USA) and Prof. P. S. Anil Kumar (IISC, Bangalore).

I want to acknowledge the Solid State and Nano Research Lab (SSNRL) at IIT Delhi, where the major part of my thesis work has been carried out. I also acknowledge the departmental X-ray diffraction facility at Dept. of Chemistry, IIT Delhi, the

departmental PPMS facility at Dept. of Physics, IIT Delhi, the Central Research Facility (CRF) and the Nano Research Facility (NRF) at IIT Delhi, and the research facilities available at INST Mohali.

I express my heartfelt thanks and great appreciation to my labmates and colleagues to make the lab environment cordial and help me whenever required. Seniors like Dr. R. Parthasarathy, Dr. Gohil S. Thakur, Dr. Zeba, Dr. Kasinath Ojha, Dr. Sandeep Dhaka, Dr. Arabinda Baruah, Dr. Nibedita Das, Dr. Vaishali Sethi, Dr. Nitin Yadav, Dr. P. Sharmila, Dr. Waseem Raza, Dr. Gajanan Kunde, Dr. Anirban Das and Dr. Kalithasan N. have always been the source of constant motivation. On the other hand, juniors like Moumita, Antara, Preeti, Shalini, Priyanka, Kirandeep, Manisha, Prabuddha, Manoj and Akshita are always full of enthusiasm and endless possibilities. A special mention for Gohil sir and Zeba ma'am for guiding and helping me to develop the skills for vacuum sealing, glove box handling, four probe resistivity measurements, and intermetallic synthesis in my early days in the lab. I want to thank Moumita for her generous help in the experimental part, while her profound scholarly background and critical analyzing skill greatly support our joint research activity. I am obliged to be a part of such an exciting research group where constant motivation, enthusiasm for research, and immediate scientific support have greatly benefitted me.

I want to thank my friends and colleagues at INST: Dimple, Ankur, Arka, Naimat, Sanjay, Rajinder, Ashmeet, Munish, Swati, Ritu, Rashmi, Devanshi, Anup, Gaurav, Anirban, Nitya, Kalpesh, Ruchi, Neha, Renu, Harmanjit, Pulkit, Sandeep, Krishna, Venu, Astha, Vipul, Nand Kumar, Vinod sir, Sanjeev sir and others, at IISER: Sudhanshu, Deepak, Avinash, Ramu, Anirban, Shailesh, Shekhar, Aslam, Ankit, Satyam, Swagatam, Vikramaditya, Pinku, Ayan and others for being a source of great joy and many of other unmentioned support during my years at INST and IISER.

I take this opportunity to convey my deepest appreciation to my close friends and part of my extended family Arup, Arnob, Gupta, Das, Koushik, Pankaj, Ujjal, Nitu, Suman, Davinder, Sanjay, Astha, Mohua, Enakshi, Piyali, Veena, Shriparna, Kathakali, Tanusree, Sudipta da, Papiya ma'am, Jayeeta, Santanu, Anurag and Nancy for being there always to support and motivate me to achieve my goals.

All of my success and achievements in life would not have been possible without the unconditional love and constant support of my family and close relatives. Words will be powerless to express the debt and gratitude I owe to my parents Subhas Chandra Ash and Abha Rani Ash, for the hardships they have gone through and the sacrifices they have made for me. I want to thank my younger brother Laxmi Kanta Ash and my sister-in-law Mohuya Ash for being a great support for me, and I convey my love and affection to my sweet little princess Mouli. Without their consistent encouragement and support in my ups and downs, I could not have achieved what I have achieved today.

Soumen Ash

Abstract

The discovery of superconductivity in 1911 by Heike Kamerlingh Onnes is one of the most significant foundations of science that leads to a number of groundbreaking research in the field of condensed matter physics. Superconductors are highly fascinating due to their exotic properties like perfect conductivity and perfect diamagnetism, and their potential for wide range applications. Discovery of superconductivity in new materials has always been subject of interest among the material scientists. Several materials are investigated to demonstrate superconductivity, of which the cuprates, iron oxipnictides and transition metal dichalcogenides are most studied systems for last few decades. Recently, a new class of $MTCh_2$ (M: Metal, T: Transition metal, Ch: Chalcogen element with M $\neq$ T) type intercalated transition metal dichalcogenide based layered superconductors like $PbTaSe_2$, $SnTaS_2$ and $PbTaS_2$ has re-established the interest in these systems. These materials apart from being superconducting also possess nontrivial topological electronic band structure that makes them strong candidates to realize novel quantum states like topological superconductors and Majorana fermions.

In this thesis we have presented the synthesis, characterization and physical properties of transition metal dichalcogenide based layered $PbNbS_2$, $PbNbSe_2$ and $SnTaS_2$ systems. Polycrystalline samples of all these compounds were prepared via solid state reaction route following the sealed tube method. This thesis introduces two new superconductors $PbNbS_2$ and $PbNbSe_2$, and also discuss the superconducting properties of polycrystalline $SnTaS_2$. All three systems crystallize in centrosymmetric hexagonal structure with space group $P6_3/mmc$, containing alternative M (= Pb or Sn) and TCh_2 (NbS_2, $NbSe_2$ or TaS_2) layers in which T atom is accommodated in the trigonal-prismatic co-ordination with Ch atoms while M occupies the octahedral site. The $PbNbS_2$ system is found to be superconducting below $T_c \sim 8.8$ K. Superconductivity in $PbNbSe_2$ is found below $T_c \sim 5.75$ K in

association with weak ferromagnetism, which is found to evolve in the close vicinity of the superconducting transition with ordering temperature $T_{FM} \sim 4.4$ K. Coexistence of superconductivity and ferromagnetism in $PbNbSe_2$ is a novel phenomenon by itself and therefore, offers a new platform to investigate exotic physics in this system. Polycrystalline $SnTaS_2$ is found to be superconducting below $T_c \sim 2.8$ K. Detailed superconducting properties and characteristic parameters are discussed by the means of transport, magnetic and thermodynamic studies. The final chapter summarizes all the major results of our investigations on the transition metal dichalcogenide based layered superconducting systems that have been discussed in the preceding chapters and gives the prospect of their future studies and potential applications.

List of Publications

Included in the thesis

1. **Soumen Ash**, Moumita Naskar, Vipin Nagpal, Ravi Shankar P. N., A. Sundaresan, Satyabrata Patnaik and Ashok Kumar Ganguli; **Superconductivity in topological nodal line semimetal $PbNbS_2$.** (*Manuscript under preparation*)

2. **Soumen Ash**, Moumita Naskar, Vipin Nagpal, Satyabrata Patnaik and Ashok Kumar Ganguli; **Superconductivity with signature of coexisting ferromagnetism in topological nodal line semimetal $PbNbSe_2$.** (*Manuscript under preparation*)

3. **Soumen Ash**, Moumita Naskar, Ravi Shankar P. N., A. Sundaresan and Ashok Kumar Ganguli; **Superconductivity and topological properties of centrosymmetric $SnTaS_2$.** (*Manuscript communicated to Supercond. Sci. Thechnol.*)

Other publications

1. **Soumen Ash**, Moumita Naskar, Premkumar Yanda, A. Sundaresan, Laxmi Chand Gupta and Ashok Kumar Ganguli; **Negative magnetization and spin glass freezing in 112-type iron pnictide $EuFeAs_2$.** (*Manuscript communicated to J. Appl. Phys.*)

2. Moumita Naskar, **Soumen Ash**, D. P. Panda, C. Viswakarma, B. K. Mani, A. Sundaresan and Ashok Kumar Ganguli; **Superconductivity in noncentrosymmetric La_3Se_4.** (*Manuscript under preparation*)

3. Antara Sarkar, Anirban Das, **Soumen Ash**, Ravi Shankar P. N. and Ashok Kumar Ganguli; **Structural and magnetic properties of $R_{0.5}Sr_{0.5}Fe_{0.5}Mn_{0.5}O_3$ (R = Gd, Nd or Pr) perovskites.** (*J. Alloys Compd. 882, 160747 (2021)*)

4. Antara Sarkar, Anirban Das, **Soumen Ash**, Ravi Shankar P. N. and Ashok Kumar Ganguli; **Investigation of structural and magnetic properties of a Ru-deficient perovskite $PrMn_{0.5}Ru_{0.3}5O_3$.** (*Manuscript communicated to Mater. Res. Bull.*)

Contents

List of Figures

List of Tables

Chapter 1

Introduction

In this chapter we provide a general introduction about the phenomenon of superconductivity. Its brief background, several characteristics and parameters are discussed in detail. An overview about the transition metal dichalcogenide (TMD) based superconductors which are the building blocks for the superconductors that we discuss in later chapters are also given.

1.1 Superconductivity

Superconductivity is an exotic phenomena in which a material poses zero electrical resistance and expulsion of magnetic flux fields from its interior when it is cooled below a certain characteristic temperature known as critical temperature (T_c). Superconductors, in normal state, are generally not a very good conductor of current. For example, Nb, Pb, Ta, Sn become superconductor at low temperature while being a better conductor Cu, Ag, Au do not show superconductivity. In normal state, superconductors may behave as a diamagnet or paramagnet, but below T_c it certainly exhibit perfect (or quite pronounced) diamagnetism.

1.1.1 Brief history

The term *Superconductivity* was first coined by Dutch physicist Heike Kamerlingh Onnes in 1911, Leiden. During his study on electronic transport properties of mercury (Hg), he found a totally unexpected and novel behavior of sudden fall in its resistance to an unmeasurably small value ($\sim 10^{-6}\ \Omega$) around 4.2 K [1]. The absence of electrical resistance below a certain temperature was then termed as superconductivity. The very next year, Onnes found that application of a sufficiently strong magnetic field can destroy the superconductivity and restore the normal state resistance even if the temperature is below its T_c. In 1913, the element Pb was found to be a superconductor with $T_c \sim 7.2$ K [2]. Several other elemental superconductors then discovered including Nb ($T_c \sim 9.2$ K) which surpassed the record critical temperature of Pb after a long years [3].

The next important finding to be discovery of another distinguishing characteristic of superconductor: the perfect diamagnetism. In 1933, Meissner and Ochsenfeld found that not only magnetic field gets excluded from entering a superconductor, due to perfect conductivity, but also the field inside a material at normal state gets expelled as it is cooled below T_c. This phenomenon is known as *Meissner effect* [4].

Discovery of Meissner effect eventually led the brothers Fritz and Heinz London in 1935 to propose two equations that explain this effect and give an estimation of penetration depth for a superconductor [5]. The next theoretical milestone achieved in 1950 with the Ginzburg and Landau theory which described superconductivity by introducing order parameter and provided a derivation for London equations [6, 7]. In the same year, H. Fröhlich made a prediction that T_c would decrease as the average isotope mass increased [8]. This effect, known as *isotope effect*, was then experimentally verified [9, 10] and provided support for the electron-phonon interaction mechanism of superconductivity.

BCS theory, the first microscopic theory of superconductivity was introduced in 1957 by J. Bardeen, L. Cooper and J. R. Schrieffer [11]. Our present understanding

of superconductivity is mainly based on the BCS theory. According to this theory, superconductivity is a microscopic phenomenon that occurs due to a condensate state of bound electron pairs, known as Cooper pairs, that carry the supercurrent and the normal and superconducting states are separated by a characteristic energy gap. The Ginzburg-Landau and London results fit well into the BCS theory. Being the most accepted theory for superconductivity BCS theory still has some limitations to properly explain the high T_c superconductivity. BCS theory explains superconductivity using the concept of cooper pairs formed from the continual exchange of phonons between two electrons due to lattice distortions. However, the theory predicts that such cooper pairs can only form below a temperature of $\sim$ 30K as too great of lattice vibrations cause too much scattering of the electrons to be able to form cooper pairs. Hence, BCS theory is limited as it only can properly explain superconductivity in low T_c superconductors.

For the next 30 years, number of alloys and compounds were extensively studied, especially the so-called $A15$ ompounds such as Nb_3Sn ($T_c \sim 18.1$ K), Nb_3Ga ($T_c \sim 20.1$ K) and Nb_3Ge ($T_c \sim 23.2$ K), which reported the highest transition temperatures till the discovery of cuprate superconductors. Apart from this, doped semiconductors (CB_x, $T_c \sim 10$ K), intercalated graphite (C_6Ca, $T_c \sim 11.5$ K), layered transition metal dichalcogenides ($NbSe_2$, $T_c \sim 7.2$ K), Chevrel phases ($PbMo_6S_8$, $T_c \sim 15$ K), magnetic superconductors ($ErRh_4B_4$, $T_c \sim 8.7$ K) were several classes of superconductors investigated before 1986.

The major breakthrough in the field of superconductivity came in 1986, when a copper oxide based layered ceramic material La-Ba-Cu-O was discovered to be a superconductor with $T_c \sim 30$ K [12]. Discovery of cuprate superconductors revolutionized the field and started the age of high-T_c superconductivity. Several cuprate superconductors were discovered within a few years with transition temperature reaching as high as $\sim$ 90 K for $YBa_2Cu_3O_{7-\delta}$ [13], $\sim$ 110 K for $Bi_2Sr_2Ca_2Cu_3O_{10}$ [14], $\sim$ 125 K for $Tl_2Ba_2Ca_2Cu_3O_{10}$ [15] and $\sim$ 133 K for $HgBa_2Ca_2Cu_3O_{8+\delta}$ [16] at ambient pressure.

In the last decade a new class of Fe-based layered superconductors gained worldwide attention. The first superconductor of this family was LaOFeP with $T_c \sim 4$ K [17], almost went unnoticed until superconductivity with $T_c \sim 26$ K was discovered in $LaO_{1-x}F_xFeAs$ by Kamihara and group [18]. Normally Fe was not considered as a good candidate for superconductivity due to its strong ferromagnetic nature, such high T_c in Fe-based compounds were therefore very unlikely. Several other families of Fe-based superconductors were then discovered within a few years, such as AEFeAsF ($CaFe_{1-x}Co_xAsF$, $T_c \sim 22$ K) [19], $AEFe_2As_2$ ($Ba_{1-x}K_xFe_2As_2$, $T_c \sim 38$ K) [20], FeSe ($T_c \sim 8$ K) [21], AFeAs (LiFeAs, $T_c \sim 18$ K) [22], $A_xFe_2Se_2$ ($K_xFe_2Se_2$, $T_c \sim 30$ K) [23] (AE: alkaline earth metals, A: alkali metals). Some other recently reported superconductors are $CaKFe_4As_4$ ($T_c \sim 33.1$ K) [24], $KCa_2Fe_4As_4F_2$ ($T_c \sim 33$ K) [25] and $RbLn_2Fe_4As_4O_2$ ($T_c \sim 35$ K) [26] (Ln: Lanthanides). The highest T_c achieved in Fe-based superconductors till now is ~ 58 K in $SmFeAsO_{1-x}F_x$ [27].

In 2012, a new class of superconductors with BiS_2 conducting layers was introduced by Mizuguchi and coworkers. Superconductivity in $Bi_4O_4S_3$ ($T_c \sim 4.6$ K) [28] and $LaO_{1-x}F_xBiS_2$ ($T_c \sim 10.6$ K) [29] led to discovery of several other BiS_2-based superconductors [30–33].

The material systems discussed in this thesis is based on the transition metal dichalcogenide superconductors $NbSe_2$ ($T_c \sim 7.2$ K) [34], NbS_2 ($T_c \sim 6.5$ K) [35] and TaS_2 ($T_c \sim 0.8$ K) [36]. Recent report of superconductivity and nodal line topology in $PbTaSe_2$ ($T_c \sim 3.8$ K) has stimulated enormous research interest [37–43]. Following the discovery of $PbTaSe_2$ isoelectronic $SnTaS_2$ [44] and $PbTaS_2$ [45] are reported lately.

Apart from all these superconductors some other important systems are there that deserve special mention viz. MgB_2 ($T_c \sim 39$ K) [46], $LnNi_2B_2C$ ($T_c \sim 16$ K) [47, 48], heavy fermion superconductors ($CePt_3Si$, $T_c \sim 0.75$ K) [49]. Recent reports on highly intruging hydride superconductors, at very high pressure the transition temperature reached to as high as 288 K, open a new avenue that possibly may lead to room temperature superconductivity in near future [50–53].

1.1.2 Perfect conductivity

The most important aspect of a material to be a superconductor is its perfect conductivity. Below a certain temperature superconductor shows practically zero electrical resistance and become a perfect conductor. This characteristic temperature is known as *critical temperature* or *superconducting transition temperature* (T_c).

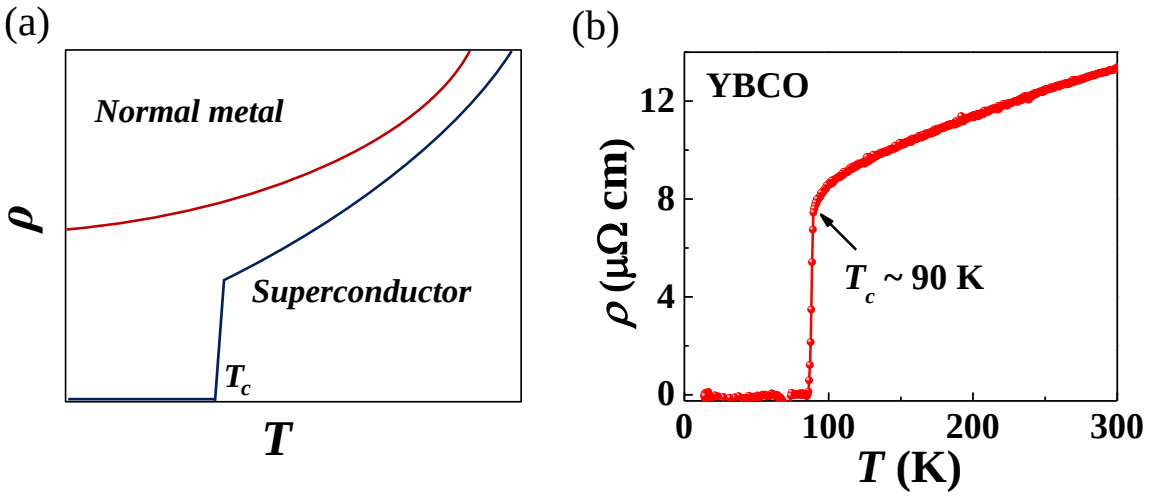

Figure 1.1. (a) Temperature dependence of resistivity for a normal metal and a superconductor. (b) Temperature dependent resistivity showing superconductivity of a $YBa_2Cu_3O_{7-\delta}$ (YBCO) sample.

Fig. 1.1(a) represents standard behaviour of a superconductor in comparison to a normal metal and Fig. 1.1(b) shows the temperature dependence of a polycrystalline $YBa_2Cu_3O_{7-\delta}$ (YBCO) superconductor that we have prepared in our lab. Electrical resistance in a material primarily arises due to the scattering of the conduction electrons by the lattices owe to their tharmal vibration. When a normal metal is cooled down much below the room temperature, the tharmal vibration of the atoms decreases. This results in decrease of the resistivity of the material, but it never reaches to zero. On the other hand, resistivity of a superconductor shows abrupt drop below its critical temperature and eventually reaches to an immeasurable value (almost zero). In superconductors, the scattering mechanism is no longer effective and thus the electrons move unimpeded through the material. The reason behind this complete loss of the resistance is not fully understood. The most

widely accepted explanation of this perfect conductivity is given by the BCS theory (1957) [11]. According to this theory, mutually linked pairs of electrons, known as *Cooper pairs*, get formed due to electron-phonon interaction and act as the carrier of the supercurrent when cooled down below the critical temperature, T_c. Due to this perfect conductivity, an electrical current set in a superconducting loop ($T < T_c$) can keep flowing indefinitely without requiring any external power source. This perpetual electric current is known as *persistent current*.

1.1.3 Perfect diamagnetism

The second hallmark characteristic for a superconductor is its perfect diamagnetism. When a superconductor is cooled down in presence of an external magnetic field, below its critical temperature T_c, it expels all the magnetic flux from its interior and behaves as a perfect diamagnet with magnetic susceptibility $\chi = -1$. This phenomenon is known as characteristic *Meissner effect*, discovered by Meissner and Ochsenfeld (1933) [4].

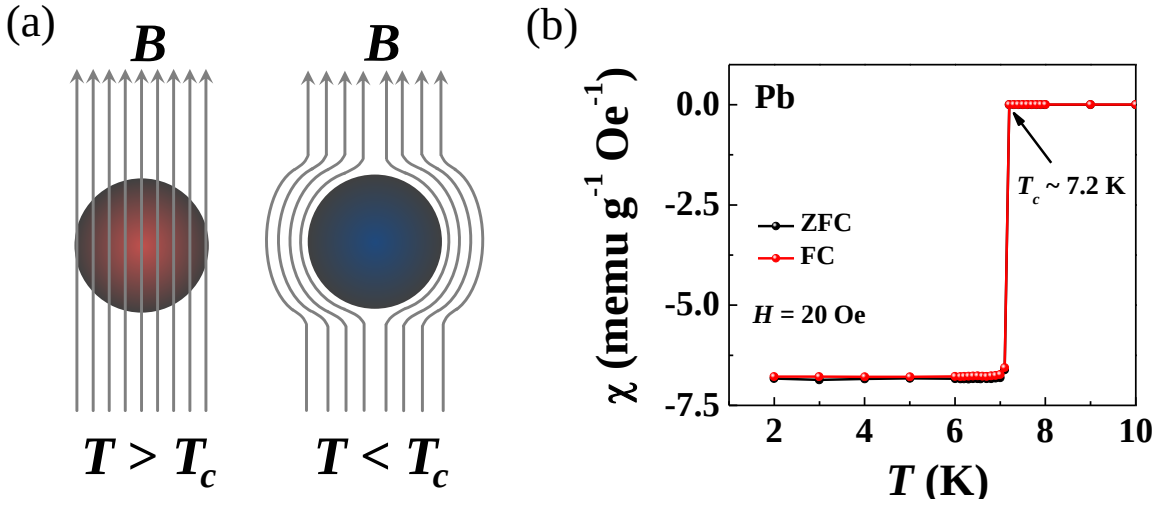

Figure 1.2. (a) Expulsion of magnetic flux from the interior of a superconductor. (b) Temperature dependent magnetic susceptibility of Pb showing Meissner effect.

Fig. 1.2(a) depicts the magnetic flux expulsion by a superconductor when cooled down below T_c. Due to the influence of an external magnetic field, a surface current develops to create magnetization which opposes the external magnetic field, resulting

in cancelling out the magnetic field from the inside of the superconductor and exhibiting perfect diamagnetism. This surface current is known as *demagnetization current* or *shielding current*. Fig. 1.2(b) shows the temperature depending zero field cooled (ZFC) and field cooled (FC) magnetic susceptibility, demonstrating Meissner effect in superconducting element Pb.

1.1.4 Type-I and type-II superconductors

Depending upon the responses to the externally applied magnetic field the superconductors are devided into two categories: *type-I* and *type-II*. For every superconductor there is a characteristic maximum magnetic field, known as *critical field* (H_c), that can be applied just before the superconductor reverts back to its nonsuperconducting state. Type-I superconductors are those which abruptly reverts back to its normal state with application of magnetic field just greater than the critical field H_c. At this stage the Meissner state vanishes and the magnetic flux lines can penetrate through the material unhindered. On the other hand, for a type-II superconductor, there is an additional intermediate state that occurs in between the Meissner state and the normal state known as *vortex state* or *mixed state*. The vortex state is a mixing of both the normal state and the superconducting state. At this stage, the magnetic flux lines are pinned in some parts of the material where normal state is stabilized, while the rest of the parts remain superconducting and exhibit Meissner effect by expelling the magnetic field. Fig. 1.3(a) and Fig. 1.3(b) show the temperature dependence of critical magnetic field for type-I and type-II superconductors respectively. Type-II superconductors are, therefore, characterized by two critical magnetic fields viz. *lower critical field* (H_{c1}) and *upper critical field* (H_{c2}). The magnetic flux lines start penetrating above H_{c1} while a weak superconducting state still survives till H_{c2} and beyond this field the system becomes nonsuperconducting.

Generally type-I superconductors are pure metals or metalloids having very low

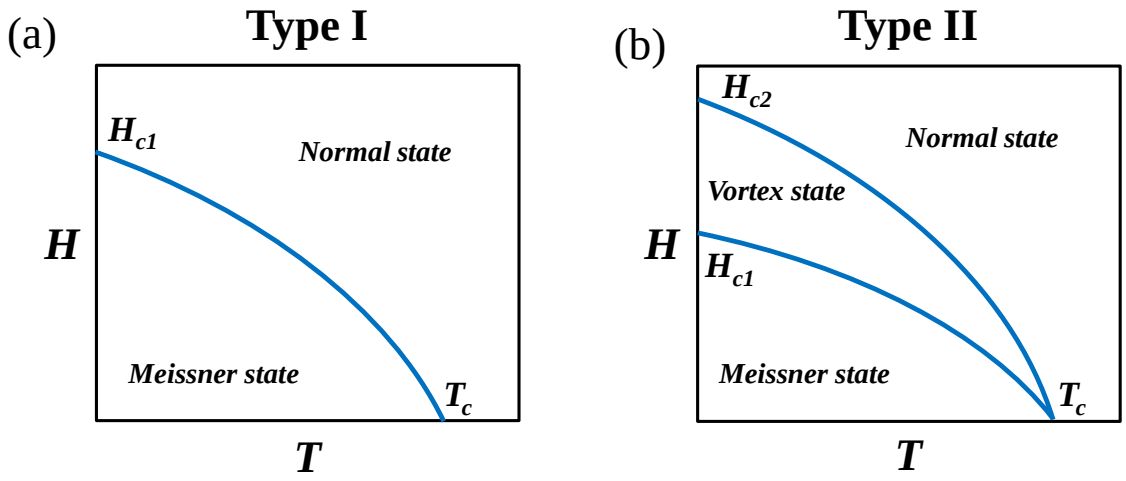

Figure 1.3. Temperature dependence of critical magnetic field for a (a) type-I superconductor and (b) type-II superconductor.

critical temperature as well as low critical field values. On the other hand, except for the elements niobium, vanadium and technetium type-II superconductors are mainly comprised of intermetallic compounds, alloys and ceramic oxides. Type-II superconductors are mostly suitable for technological applications due to their comparatively high transition temperature and higher critical field values.

1.1.5 Parameters to define a superconductor

Not only the superconducting transition temperature but also few more parameters play important roles in the behaviour of a superconductor and are required to be known for its practical applications. Here, we will discuss about some important superconducting parameters required to define the superconductivity of a material.

Critical temperature

Superconductivity is a phenomenon that usually can be observed at very low temperatures. The particular temperature below which a material undergoes a phase transition and shows superconductivity is known as its *critical temperature* (T_c).

The critical temperature is the most important parameter to define the nature

of a superconductor. Generally, superconductors having T_c below 30 K are known as *low-T_c superconductors* and those are having T_c above it are known as *high-T_c superconductors*. Some consider the boiling point of nitrogen (= 77 K) as the limiting scale to define high-T_c or low-T_c superconductors, to give emphasize whether one can cool the sample with liquid nitrogen or not.

Critical field

Apart from the limitation of having a maximum operating temperature (T_c), superconductivity can also be destroyed by applying a sufficiently large magnetic field, known as *critical field* (H_c). Type-I superconductors have only one critical field (H_c) value while type-II superconductors are defined by two characteristic critical field values: lower critical field (H_{c1}) and upper critical field (H_{c2}).

Variation of the critical magnetic field with temperature is shown in Fig. 1.3. Nature of the temperature dependent critical field (lower critical field in case of type-II superconductor) can be approximated well by the formula:

$$H_{c1}(T) = H_{c1}(0)[1–(T/T_c)^2] \tag{1.1}$$

On the other hand, temperature dependence of the upper critical field for a type-II superconductor can be fitted well with generalized Ginzburg-Landau (GL) formula:

$$H_{c2}(T) = H_{c2}(0)(1–t^2)/(1+t^2) \tag{1.2}$$

where $t = T/T_c$. At the same time, the orbital contribution to the upper critical field can be given by the Werthamer-Helfand-Hohenberg (WHH) formula:

$$H_{c2}^{orb}(T) = -AT_c(dH_{c2}/dT)_{T=T_c} \tag{1.3}$$

where $A = 0.69$ or 0.72 for the dirty and clean limits respectively [54].

The external magnteic field that will be strong enough to break the Cooper pairs

and destroy the superconductivity is theoretically determined by the *Pauli limiting field* or *Clogston-Chandrasekhar limit* defined as:

$$H_P = \Delta/\sqrt{2}\mu_B \tag{1.4}$$

where $\Delta = E_g/2$; $E_g = 3.53k_BT_c$ is the superconducting BCS energy gap ratio and μ_B is the Bohr magneton, gives $H_P = 1.85T_c$ [55, 56].

Critical current density

The current density associated with the maximum current that can be carried by a superconducting wire is known as the *critical current density* (J_c). Due to the flow of the transport current, a corresponding magnetc field gets induced to the superconductor. This induced magnetic field can achieve the critical field value H_c as the current density reaches to J_c and eventually destroys the superconductivity. This phenomenon is known as the *Silsbee effect*. The relation between the critical magnetic field and the critical current density can be expressed as:

$$H_c(T) = \mu_0\lambda(T)J_c(T) \tag{1.5}$$

where μ_0 is the permeability of vacuum and λ is the penetration depth. Temperature dependence of critical current density can be well approximated as:

$$J_c(T) = J_c(0)[1–(T/T_c)^2] \tag{1.6}$$

Coherence length

The superconducting order parameter changes with distance in the neighborhood of the boundary of a superconductor, and this provided us the first fundamental length scale of superconductivity: the coherence length ξ.

In relation to the Fermi velocity (v_F) of the material and the energy gap (E_g) associated to the condensation of the superconducting state, the coherence length

can be represented as:

$$\xi = \frac{-2\hbar v_F}{\pi E_g} \tag{1.7}$$

where $\hbar$ is the reduced Planck constant.

The superconducting coherence length is the minimum distance over which the superconducting electron density changes significantly. From the Ginzburg-Landau theory, coherence length can be estimated as:

$$\xi = \left(\frac{\Phi_0}{2\pi H_{c2}}\right)^{1/2} \tag{1.8}$$

where $\Phi_0 = h/2e$ and H_{c2} is the upper critical field.

Penetration depth

The second of the two fundamental length scales of superconductivity is the penetration depth λ. Superconducting penetration depth or the London penetration depth is associated to the exponential decay of the magnetic field at the interior surface of a superconductor when kept in an external magnetic field. The characteristic distance to which a magnetic field becomes equal to e^{-1} times that of the magnetic field at the surface of the superconductor is known as the penetration depth.

Therefore, the variation of the magnetic field (H) inside a superconductor with the distance (x) from its surface can be represented as:

$$H(x) = H_0 e^{-x/\lambda} \tag{1.9}$$

London theory gives an explicit formula for the penetration depth (λ) in relation to the density of superconducting electrons (n_s) as:

$$\lambda = \left(\frac{m}{\mu_0 n_s e^2}\right)^{1/2} \tag{1.10}$$

where m is the mass of the charge carrier with electronic charge e and μ_0 is the permeability of the free space.

On the other hand, the relation between the lower critical field (H_{c1}) and the superconducting penetration depth (λ) is given by the Ginzburg-Landau theory as:

$$\mu_0 H_{c1}(0) = \left(\frac{\Phi_0}{4\pi\lambda^2}\right) ln(\lambda/\xi) \tag{1.11}$$

where $\Phi_0 = h/2e$ and ξ is the superconducting coherence length.

Charge density wave (CDW)

Charge density wave (CDW) is a periodic modulations of conduction electron density with association of lattice distortions in solids [57–60]. It is a type instability of coupled electronic-lattice, occurred in several quasi low dimensional systems, including layered transition metal dichalcogenides. The reason behind such instability is the reduction in electrons' energy in a material as a consequence of generating a spontaneous periodic modulation of the crystalline lattice with an appropriate wave vector. The symmetry of CDW state depends upon the electronic structure of the host material. One of the most studied transition metal dichalcogenide $NbSe_2$ exhibits both CDW and superconductivity at low temperatures. In bulk 2H-$NbSe_2$, CDW order appears below 33.5 K [61] and superconductivity emerges when the temperature is lowered further below 7.2 K [62]. For 2H-TaS_2, CDW transition appears $\sim$ 80 K [63].

1.2 Superconductivity in pristine and intercalated TMDs

Transition metal dichalcogenides (TMDs) form a number of quasi-two-dimensional layered compounds that exhibit interesting and unusual physical properties. Transition metals from Group-IV, V and VI (denoted by T) with chalcogen atoms S, Se and Te (denoted by Ch) form the compounds that share common TCh_2

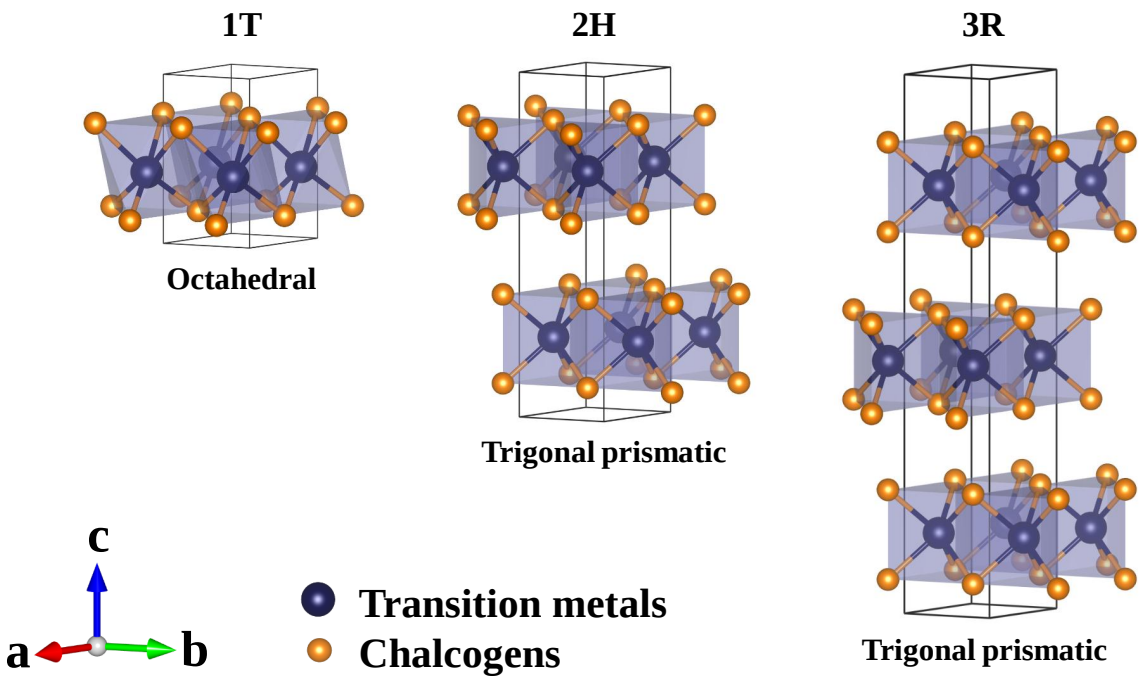

Figure 1.4. Crystal structure for polytypes of TMDs: 1T (octahedral coordination, one Ch-T-Ch unit in a unit cell), 2H (trigonal prismatic coordination, two Ch-T-Ch units in a unit cell) and 3R (trigonal prismatic coordination, three Ch-T-Ch units in a unit cell).

stochiometry. The weak van der Waals interlayer bonding between the hexagonal layers of octahedral or trigonal prismatic Ch-T-Ch building blocks allows many polytypes to form. In the octahedral configuration, the Ch-T-Ch near-neighbour group forms a straight line at a 45-degree angle with the vertical direction, whereas in the trigonal prismatic configuration, the pair of chalcogen atoms nearest to a given metal atom are displaced vertically in the c-axis direction from each other, and the metal ion is displaced horizontally form the line connecting the chalcogens. Fig. 1.4 depicts three most common polytypes 1T, 2H and 3R TMD structures in which the number 1, 2 and 3 refer to the number of TCh_2 layers in the unit cell, whereas the letter T, H and R stand for trigonal, hexagonal and rhombohedral, respectively [64,65]. 1T polymorph consists one octahedrally coordinated Ch-T-Ch layer in a unit cell, whereas 2H and 3R polymorphs are stacking arrangement of two and three Ch-T-Ch layers, respectively, with trigonal prismatic coordination.

Pristine TMDs

TMDs are found to exhibit strongly competing effects of charge-density wave (CDW) formation and superconductivity (SC). A number of Group-V TMD compounds, having TCh_2 composition, are known to be superconducting with T = Nb or Ta and Ch = S, Se or Te. The electronic properties of two TMD materials are generally quite different and depend upon the polymorhic configuration of the system. Pristine 1T polytypes, such as 1T-TaS_2, 1T-TiS_2, 1T-$TiSe_2$ and 1T-VSe_2 were never found to be superconducting at ambient pressure [66–68], while the normal state nature were found to be either semiconducting or semi-metallic. 1T-TaS_2 becomes superconducting under the influence of 2 GPa pressure and with further increase in pressure, both the Mott phase and nearly commensurate CDW are suppressed to give rise of SC with $T_c \sim 5$ K for pressure up to 25 GPa [67]. Pristine 1T-$TiTe_2$ exhibits pressure driven superconductivity at ~ 5 GPa that rapidly reaches to $T_c \sim 5.3$ K at 12 GPa and the SC state surprisingly persists even after decompression of the system down to ~ 0.5 GPa [69]. Recent report shows pressure induced suppression of CDW in 1T-VSe_2 and emergence of SC at ~ 15 GPa with $T_c \sim 4$ K [70]. Pressure induced superconductivity can also be seen in WTe_2 [71] and $MoTe_2$ [72] where WTe_2 achieve the maximum $T_c \sim 7$ K at 16.8 GPa, while $MoTe_2$ become superconducting at ~ 11.7 GPa with $T_c \sim 8.2$ K.

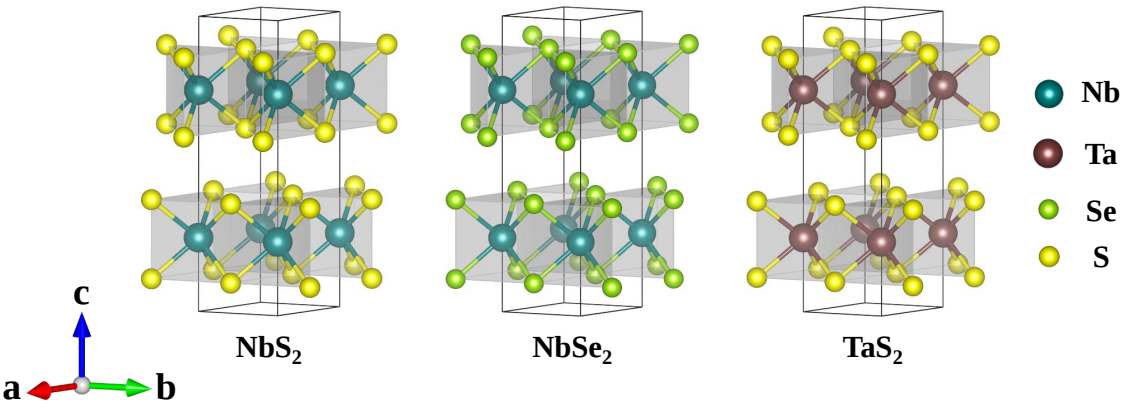

Figure 1.5. Crystal structure of 2H-type NbS_2, $NbSe_2$ and TaS_2 showing trigonal prismatic coordination and two Ch-T-Ch units in each unit cell.

Fig. 1.5 shows crystal structures for 2H polytypes of NbS_2, $NbSe_2$ ans TaS_2, consist trigonal prismatic Ch-T-Ch building blocks. In the 2H polytypes of TMDs, the transport properties are considerably more varied than in the 1T-TMDs. Ambient SC, usually assisted by CDW, is most likely to be observed in 2H-TMDs. A weak first-order CDW transition at $T_{CDW} \sim 75$ K is found to be associated with superconductivity at ambient pressure with $T_c \sim 0.6$ K in 2H-TaS_2 system [73–75]. An incommensurate CDW can be seen to form below ~ 125 K in 2H-$TaSe_2$ that bocomes commensurate with the lattice below ~ 90 K. 2H-$TaSe_2$ undergoes a superconducting transition below $T_c \sim 0.2$ K and hence commensurate CDW and SC coexist below this temperature [76–78].

2H-NbS_2 is one of the most interesting as well as quite unusual TMD system having superconducting $T_c \sim 5.84$ K with no signature of CDW transition [79–85]. The star-shaped CDW which was evident for analogous 2H-$NbSe_2$ [86, 87] is not observed in the scanning tunneling microscopy (STM) study of 2H-NbS_2 [84]. However, two superconducting gaps which are usually associated with the CDW formation in TMDs are found in the STM. This phenomenon is comparable to the cases for MgB_2 and pnictide superconductors [88]. Applying hydrostatic pressure of ~ 20 GPa the superconducting T_c was raised from 6 K to 8.9 K [85].

The best characterized superconducting TMD is 2H-$NbSe_2$ [68, 76, 78, 80, 81, 86, 89–106]. There are several aspects of 2H-$NbSe_2$ that make it highly interesting and vastly studied pristine TMD superconductor. It has the highest T_c of ~ 7.2 K for the class of pristine TMD superconductors. There is an incommensurate CDW with $T_{CDW} = 35$ K that coexist with the anisotropic superconductivity in a hexagonal crystal structure of 2H-$NbSe_2$. Direct evidence for the coexisting SC and CDW was reported by Hess [86, 107]. Moreover, growing a large size single-phase single crystal of 2H-$NbSe_2$ is comparatively easy as polytypism in the Nb-Se system is less likely than in the analogous Ta-S, Ta-Se and Nb-S systems. Application of external pressure suppresses the CDWs, as T_{CDW} decreases linearly with increasing pressure [102] and raises the superconducting T_c up to about 8.5 K [81, 98, 102].

Metal intercalated TMDs

CDWs in TMDs usually get suppressed by application of external pressure or by intercalation, resulting SC to enhance, even in the 1T polytypes. We can categorize the metal intercalated superconducting TMDs into two classes. The first class represents the set of superconducting Group-V TMD materials intercalated with a transition metal. This class is having the common composition of M_xTCh_2 with M $\neq$ T as a transition metal. Almost all the transition metals can be intercalated into these Group-V TMDs by following the reaction conditions similar for the pristine compounds. A small amount of intercalate is sufficient to increase the *c*-axis and to affect significantly its physical properties. 2H-$Co_{0.075}NbSe_2$ and 2H-$Fe_{0.05}TaS_2$ were prepared by adding a small amount of M to the starting material [108]. The concentration of the ferromagnetic metal intercalant within the TCh_2 layers is not sufficient to suppress the superconducting T_c to zero, as in the pair-breaking theory of Abrikosov and Gor'kov (1961) [109]. Surprisingly, the T_c of 2H-$Fe_{0.05}TaS_2$ greatly exceeds that of 2H-TaS_2 itself. The competition between CDW and superconductivity in Cu_xTaS_2 was studied by Wagner *et.al.* [110]. Transport, magnetic and thermal properties measurements for various x values were carried out, and the maximum T_c of 4.7 K was found for x = 0.04. A phase diagram was presented by including both the CDW transition temperature and the superconduccting T_c as functions of Cu concentration. Superconducting $MxTaS_2$ type intercalation compounds of 2H-TaS_2 were prepared with x = 1 using transition metals Hg, In, Sn and Pb had T_c of 2.1 K, 1.0 K, 2.95 K and 1.7 K, respectively [111, 112], while for M = Bi the x compositions 1/3 and 2/3 were synthesized with superconducting T_c of 2.0 K and 0.78 K, respectively [111].

The second class of metal intercalated TMD compounds generally associates intercalation of the Group-IV and VI TMD compounds with alkali or alkali earth metal. These materials were synthesized by first preparing the dichalcogenide using vapour-phase transport, and then the intercalation can be achieved mainly in three

ways: by exposing the TCh_2 to the alkali vapour, exposing it to the alkali or alkali earth element dissolved in liquid ammonia and then evaporating the excess ammonia, and by reacting it with n-butyllithium in hexane. CDWs are generally removed via intercalation with a large variety of elements or compounds, and the resulting superconductors are often extremely anisotropic in their normal and superconducting state properties. Number of layered superconductors were prepared by doping (or intercalating) 2H-MoS_2, 2H-TaS_2, 1T-TaS_2, 2H-ZrS_2, and 2H-$ZrSe_2$ TMDs with alkali metals [113–118]. The resulting superconducting compounds were very air-sensitive. Superconductivity can be induced into 2H-MoS_2 with $T_c \sim 11$ K by electrostatic gating [119]. Ye *et.al.* discuss the unified phase diagram of superconductivity for both electrostatically and chemically doped 2H-MoS_2 as a function of alkali metal doping concentration and carrier density. A very interesting superconducting system is Cu_xTiSe_2, prepared and studied by Morosan *et.al.* [120]. The pristine $TiSe_2$ is either a semimetal or a semiconductor due to a commensurate CDW. Intercalation of Cu into the $TiSe_2$ layers supressed the charge-density wave and the materials become superconducting with the maximum $T_c = 4.15$ K attained for x = 0.08.

1.3 Motivation and structure of the thesis

Discovery of new superconductor and study of its exotic physics have always been of great interest among the material scientists. Metal intercalation in quasi-2D layered structure of TMD is a very effective approach, that may lead to interesting properties such as suppression of CDW, evolution of superconductivity or sometimes enhancement of superconducting T_c. Recent discovery of nodal line superconductivity in noncentrosymmetric $PbTaSe_2$ has renewed the interest in the intercalated transition metal dichalcogenide based layered systems [37, 40]. Related isoelectronic systems such as $PbNbSe_2$, $SnTaSe_2$, $SnNbSe_2$ and $PbTiSe_2$ are theoretically predicted to be superconducting [121, 122]. After $PbTaSe_2$, superconducting properties of centrosymmetric $SnTaS_2$ [44] and $PbTaS_2$ [45] have been studied in details in the

single crystal form, focussing on their possible topological characteristics. We were already working on the study of superconducting properties in our polycrystalline $SnTaS_2$ sample when these two reports came.

In this thesis we have discussed the synthesis, characterization and physical properties of metal intercalated transition metal dichalcogenide based $PbNbS_2$, $PbNbSe_2$ and $SnTaS_2$ systems. $PbNbS_2$ and $PbNbSe_2$ have been introduced here as two new superconductors, while we also discuss the superconducting properties of polycrystalline $SnTaS_2$.

The thesis has been divided into six chapters as follows:

Chapter 1: Introduction.

Chapter 2: Experimental techniques.

Chapter 3: Superconductivity in $PbNbS_2$.

Chapter 4: Superconductivity and ferromagnetism in $PbNbSe_2$.

Chapter 5: Superconductivity in $SnTaS_2$.

Chapter 6: Summary and future outlook.

Chapter 1: Introduction

In the first chapter, a general introduction of superconductivity and its brief background have been presented. Key superconducting characteristics and parameters are explained. Structural and physical properties of the pristine and intercalated transition metal dichalcogenide based superconductors have been discussed. A detailed literature survey and the motivation for the thesis have been presented.

Chapter 2: Experimental techniques

In the second chapter, detailed synthesis procedure to acquire polycrystalline samples of $PbNbS_2$, $PbNbSe_2$ and $SnTaS_2$ has been discussed. An overview of solid state reactions, sealed tube method and intercalation technique are presented. Several characterization techniques and the measurement criteria that have been used to

study the physical properties of the materials under consideration are discussed in detail.

Chapter 3: Superconductivity in $PbNbS_2$

In the third chapter, we have reported transition metal dichalcogenide based layered superconductor $PbNbS_2$. Synthesis, crystal structure, electrical resistivity, magnetic susceptibility and heat capacity of polycrystalline $PbNbS_2$ have been studied in detail. $PbNbS_2$ crystallizes in a centrosymmetric hexagonal structure consist of alternating Pb and NbS_2 layers which separated by weak van der Waals force. The system is found to be superconducting below $T_c \sim 8.8$ K. Detailed superconducting properties and characteristic parameters are discussed by the means of transport, magnetic and thermodynamic studies.

Chapter 4: Superconductivity and ferromagnetism in $PbNbSe_2$

In the fourth chapter, we discuss another transition metal dichalcogenide based layered superconductor $PbNbSe_2$. Synthesis, crystal structure, electrical resistivity and magnetic properties have been studied in detail. $PbNbSe_2$ crystallizes in a centrosymmetric hexagonal structure with alternative Pb and $NbSe_2$ layers separated by weak van der Waals force. $PbNbSe_2$ is found to be superconducting with $T_c \sim 5.75$ K. Detailed transport and magnetic properties have been discussed. A weak ferromagnetism is found to evolve in the close vicinity of the superconducting transition with ordering temperature $T_{FM} \sim 4.4$ K. Coexistence of superconductivity and ferromagnetism in $PbNbSe_2$ is a novel phenomenon.

Chapter 5: Superconductivity in $SnTaS_2$

In the fifth chapter, we have presented the detailed physical properties study of transition metal dichalcogenide based $SnTaS_2$ superconductor. Superconductivity in $SnTaS_2$ was known from 1970 but lacked a detailed study of its physical properties. We have discussed the synthesis, crystal structure, electrical transport properties and magnetic properties of polycrystalline $SnTaS_2$ in detail. The material crystallizes in a centrosymmetric hexagonal structure consist of alternative van der Waals layers of

Sn and TaS_2. Polycrystalline $SnTaS_2$ is found to be superconducting below $T_c \sim 2.8$ K. Key superconducting parameters are discussed in detail.

Chapter 6: Summary and future outlook

The sixth and final chapter summarizes the major findings of our investigations on the transition metal dichalcogenide based layered superconducting systems that have been discussed in the preceding chapters of this thesis, and gives the prospect of the future studies.

Chapter 2

Experimental techniques

In this chapter we describe the synthesis and characterization techniques that are used for preparing and carrying out physical properties studies of the material systems discussed in this thesis.

2.1 Synthesis

2.1.1 Solid state reaction

The most extensively used technique to synthesize polycrystalline materials is the solid state reaction method. As the name suggests, this synthesis route involves a reaction of two or more solid components. It is quite obvious that such a reaction will not be completed in any reasonable time scale at room temperature. It is therefore required to heat them at high temperatures, typically above $\sim$ 800 °C. Generally, the solid reactants are not raised to their melting point, so the reaction takes place in the solid state (subsolidus). The reaction may proceed very slowly, but increasing the temperature can accelerate the reaction by increasing the diffusion rate. At these high temperatures, the reaction, between the thoroughly mixed starting materials, happens through diffusion and still takes several days and requires several such heat treatments to get a phase pure sample.

Some measures are need to be taken for a solid state reaction: (1) The reactants must be taken in stoichiometric ratio. (2) Based upon the reactivity of reagents, different crucible and environment need to be considered. (3) The starting materials must be ground thoroughly in an agate mortar and pestle, typically for about an hour, to increase the surface area that will speed up the diffusion process. (4) To promote proximity of reagents, one can press the starting mixture into pellets by applying a pressure of typically ~ 5 tonnes. (5) The mixed powder/pellets have to be given high temperature heat treatments for several days with intermediate grinding. Some drawbacks that may be identified are non-uniformity of particle size and shape, multiphase character, lack of reproducibility and loss of stoichiometry.

2.1.2 Sealed tube method

The most conventional method for preparing intermetallic compounds which are often air sensitive is reaction of solid reactants at high temperature for several hours in a sealed quartz ampoule. The reactants are weighed in stoichiometric amounts and mixed together in an inert atmosphere (inside a nitrogen/helium/argon filled glove box). The mixture then finally ground together either manually with mortar and pestle or by ball milling. This mixture further can be cold pressed for a better compactness and then flame sealed in an evacuated quartz tube (pressure $< 10^{-5}$ mbar). The quartz ampoule is then heated at desired temperature. As the temperature rises and reaction precedes the surface area of the reactant decreases. The effect of grinding is to ensure a high surface area and an intimate mixing between the reactants. Information about the phase diagram of the reactants serves as a guideline in designing the reaction conditions and compositions for synthesis. Often, the reactants can attack quartz tube during the course of reaction and pose several problems like inclusion of secondary phases, difficulty in product separation or cracking of tubes. To overcome these problems the reactants are kept inside alumina or other inert crucible or are sealed in a metal tube (Nb or Ta) before sealing in

quartz tubes. The choice of type of crucible depends on the initial reactants.

2.1.3 Intercalation technique

One of the most effective technique to tune the physical properties of layered transition metal dichalcogenides (TMD) is the metal intercalation approach. The term *intercalation* literally means the process of including some extra time period into the calendar, such as February 29 in a leap year. In chemistry, it refers to the reversible insertion of guest species into the layeres of a host crystal without destroying the structural features of the host. Fig. 2.1 depicts the intercalation process, in which the intercalants get inserted into the interlayer spaces of the host material.

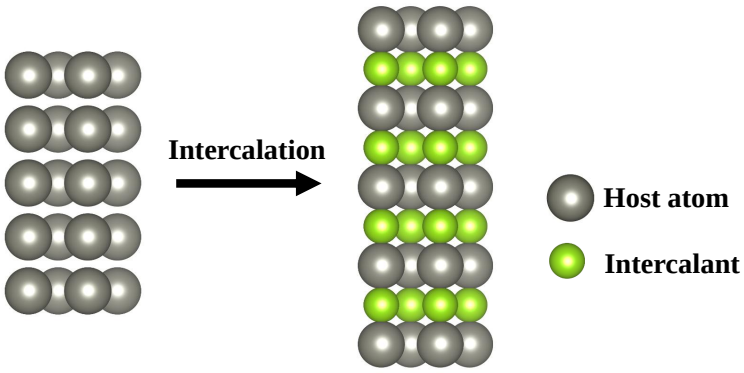

Figure 2.1. Intercalation technique showing the insertion of intercalate atoms into the layers of the host crystal structure.

In TMD, from alkali metal ions to post-transition metal ions can be used as intercalates, which can significantly affect the structural, chemical, electronic, magnetic or optical properties of the host material. Typically, intercalation facilitates the charge transfer between the guest ions and the host material that eventually induces structural changes as well as markedly affect the conductivity behaviour of the system depending on the degree of electron transfer between guest and host layers.

Successful Pb intercalation into the van der Waals (vdW) layers of 2H-NbS_2 and 2H-$NbSe_2$ was achieved via solid state reaction routes to synthesize polycrystalline $PbNbS_2$ and $PbNbSe_2$. Similarly, Sn intercalation into the vdW layers of 2H-TaS_2 was carried out by solid state reactions which led to formation of polycrystalline $SnTaS_2$.

2.1.4 Polycrystalline $PbNbS_2$, $PbNbSe_2$ and $SnTaS_2$

We now describe the synthesis details of the specific materials studied in this thesis. Polycrystalline samples of $PbNbS_2$, $PbNbSe_2$ and $SnTaS_2$ were synthesized via solid state reaction route following a sealed tube method approach. The deatil reaction protocols are discussed below.

$PbNbS_2$

Polycrystalline $PbNbS_2$ was prepared from the solid state reaction of elemental Pb with presynthesized NbS_2. First, NbS_2 precursor was synthesized from the reaction of Nb turnings (Aldrich, 99.8%) and S powder (Sigma Aldrich, 99.98%). Stoicheometric amount of Nb metal and S powder were taken, ground well then sealed in an evacuated quartz tube and heat treated at 850 °C for 48 h. Next, Pb granules (Acros, 99+%) and prereacted NbS_2 powder were taken into stoicheometric ratio and further mixed and ground thoroughly. The mixture was then vacuum sealed in a quartz tube and heated at 800 °C for 7 days and then cooled down to the room temperature by switching off the furnace. The heat treated sample was then reground, pelletized and again sealed in an evacuated quartz ampoule followed by sintering at 800 °C for another 7 days and then furnace cooled to the room temperature. The final product is dark grey in colour and having a metallic lustre. The air-stable sample is kept in an argon filled glove box to prevent any unwanted contamination. The entire sample handling except pelletizing and sealing was carried out inside a glove box with controlled oxygen and moisture atmosphere (maintained concentration is < 0.1 ppm for each).

$PbNbSe_2$

Polycrystalline $PbNbSe_2$ was synthesized via solid state reaction route taking Pb, Nb and Se in elemental form. Pb granules (Acros, 99+%), Nb powder (Acros, 99.8%) and Se powder (Alfa Aesar, 99+%) were taken in stoicheometric ratio, ground thoroghly and then sealed in an evacuated quartz ampoule. The sealed reactants were then

heated at 850 °C for 48 h and then cooled down to room temperature with a cooling rate of 100 °C/h. The heat treated mixture was then reground, pelletized and resealed in an evacuated quartz tube. The sample was then sintered at 850 °C for 48 h and finally cooled down to the room temperature following a 100 °C/h cooling rate. The final product is dark grey in colour with metallic lustre. The sample is air-stable but preserved in an argon filled glove box to avoid any possible contamination. All the sample handling except pelletizing and sealing were performed inside an argon filled glove box under controlled oxygen and moisture level (< 0.1 ppm each).

$SnTaS_2$

Polycrystalline $SnTaS_2$ was synthesized via solid state reaction route taking elemental Sn and presynthesized TaS_2 in stoicheometric ratio. First, TaS_2 precursor was prepared by reacting stoicheometric amount of Ta powder (Alfa Aesar, 99.9%) and S powder (Sigma Aldrich, 99.98%) at 850 °C for 48 h in a vacuum sealed condition. Next, this TaS_2 powder was mixed with Sn granules (Sigma Aldrich, 99.5+%) and ground thoroghly. The mixture was then sealed in an evacuated quartz tube, heat treated at 850 °C for 48 h and cooled down to room temperature by following a cooling rate of 150 °C/h. The sample was then reground, pelletized and resealed in an evacuated quartz tube followed by sintering at 850 °C for 48 h. The sample was then cooled down to room temperature with 150 °C/h cooling rate. The air stable sintered sample is dark grey in colour with a metallic lustre. To avoid any unwanted contamination the sample was preserved in an argon filled glove box with a controlled atmosphere (oxygen and moisture level is < 0.1 ppm). All the sample handling except vacuum sealing and pelletizing were carried out inside the glove box.

2.2 Characterization

2.2.1 X-ray diffraction

Powder X-ray diffraction is a powerful and widely used technique to determine the crystal structure as well as phase purity of a crystalline material. X-ray is an electromagnetic radiation having wavelength comparable to the interatomic distances in the crystalline solids. A single crystal can be devided into various sets of parallel atomic planes that can act as a three dimensional grating for X-rays. After getting reflected by these sets of parallel atomic planes X-rays result into a diffraction pattern by following the Bragg's law for constructive interference,

$$2dsin\theta = n\lambda \tag{2.1}$$

where d is the inter-planar distance between the (hkl) planes, λ is the wavelength of the incident X-ray beam, θ is the scattering angle and n is a positive integer giving the order of reflection $(n = 1, 2, 3, ...)$ [123].

The phase purity of all the samples discussed in this thesis were characterized by room temperature powder X-ray diffraction technique using a Bruker D8 Advance diffractometer with Cu-Kα radiation source and Ni-filter. Structural analysis has been performed by Rietveld refinement method with a least square fitting approach using TOPAS 4.0 software package [124]. A shifted Chebyschev polynomial of first kind with 10 variables was used for background modelling and the shape of peaks were described by Thompson-Cox-Hastings pseudo-Voigt function.

2.2.2 Resistivity

Temperature dependent electrical resistivity in the range of 2 – 300 K was measured in a cryogen free transport properties measurement set up (Cryogenics Ltd.) using a standard four-probe technique. In a four probe measurement, four point contacts are made on a freshly cleaved surface of the sample pellet, a constant current I ($\sim$ 10

mA) is applied to the outer probes and potential difference V is measured across the inner probes. Fig. 2.2 depicts the schematic, as well as the practical realization of four probe contact.

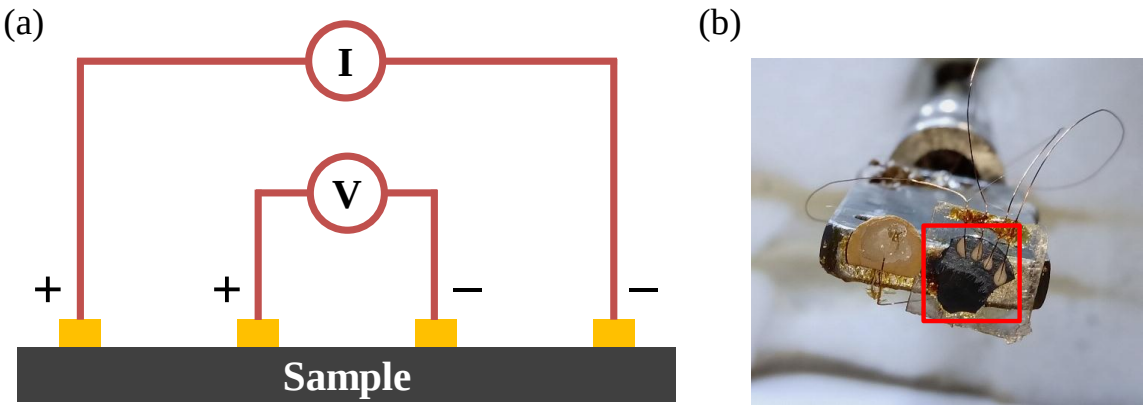

Figure 2.2. (a) Schematic diagram of four probe point contact geometry used for resistivity study. (b) Picture of four probe point contact made on a polycrystalline sample loaded on a sample holder.

The inner probes draw very small current (ideally no current) because of the high impedance of the voltmeter. Thus unwanted voltage drop at the contacts due to contact resistance between probes and the sample is eliminated from the voltage measurement. The resistivity ρ of the sample is obtained from a voltage V measurement at constant current I using the Ohm's law:

$$\rho = \left(\frac{VA}{IL}\right) \tag{2.2}$$

where A is the cross-sectional area of the sample through which current passes, and L is the distance between the two voltage leads.

Field dependence of the resistivity was studied by applying external magnetic field ranging from 0 – 1 T perpendicular to the probe current direction.

2.2.3 Magnetism

Temperature dependent and field dependent magnetic measurements were performed in a superconducting quantum interference device (SQUID, Quantum Design

MPMSXL-7 T). Both zero field cooling (ZFC) and field cooling (FC) protocols were followed for the temperature dependent DC susceptibility measurement whereas field dependence of magnetization was studied in the zero field cooling condition. To diminish the remanent field, a demagnetization sequence was run at room temperature before measuring the magnetism in the superconducting state. The magnetic field was ramped up to maximum (= 7 T), then to the maximum in the opposite direction (= − 7 T). The field was roughly halved at each subsequent step and the positive and negative direction was repeated down to 10 Oe, then finally to zero.

2.2.4 Heat capacity

Temperature-dependent heat capacity for representative samples was measured in a physical properties measurement system (Quantum Design PPMS-7 T) under zero field and applied magnetic field down to 2 K. The heat capacity option in the QD-PPMS uses a relaxation technique (QD, 2004).

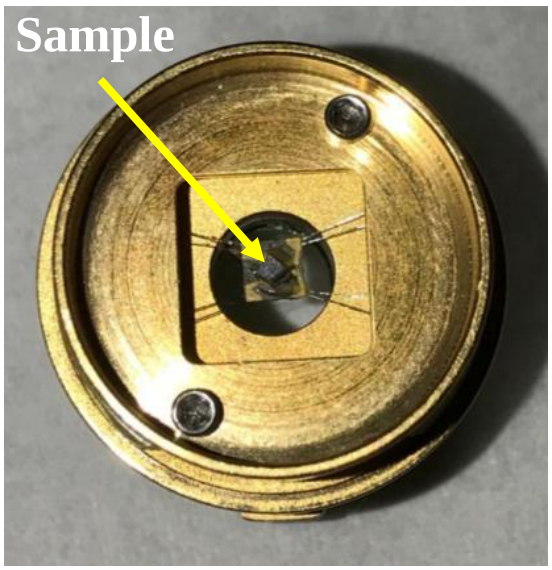

Figure 2.3. Superconducting sample loaded onto a heat capacity measurement platform.

As shown in Fig. 2.3, the samples were attached to the heat capacity platform which contains a heater and a thermometer with a thin layer of Apiezon N grease. The platform is connected through conducting wires to a reservoir. After the bath

and the sample have reached the same temperature, a well defined constant heating pulse is applied to the platform for a fixed time (heating process), until a steady state temperature is reached. The heater power is then turned off and the temperature decays for the time duration. After each measurement cycle (a heating process and a cooling process), the heat capacity values can be obtained by fitting the entire temperature response of the sample platform to a model which includes both thermal relaxation of the sample platform to the bath temperature and the thermal relaxation between the platform and sample itself.

Chapter 3

Superconductivity in $PbNbS_2$

3.1 Introduction

2H-NbS_2 with a quasi-2D structure shows superconductivity below $T_c \sim 5.84$ K [79–85]. It is a metal in the normal state and there is no signature of CDW transition in NbS_2. Absence of CDW is a quite uncommon feature for a transition metal dichalcogenide system. It consists layered NbS_2 units in which Nb atoms occupy the trigonal prismatic position coordinated by S atoms (Fig. 1.5). These layers are strongly associated in the *ab*-plane due to covalent bonding, while stacked together along the *c*-axis by weak van der Waals interaction. Due to this weak van der Waals force metal ions can be easily intercalated into the NbS_2 layers, resulting significant changes in its crystal structure as well as electronic properties.

Polycrystalline $PbNbS_2$ has been prepared by following metal intercalation approach via solid state synthesis route. Structural, transport, magnetic and thermodynamic properties have been studied. $PbNbS_2$ crystalizes in centrosymmetric hexagonal structure with space group $P6_3/mmc$. $PbNbS_2$ is found to be a superconductor with $T_c \sim 8.8$ K. Superconducting T_c has increased due to intercalation effect. Important superconducting parameters such as upper and lower critical fields, coherence length, penetration depth, Ginzburg-Landau parameter, thermodynamic critical field, Debye temperature, and nature of spin-orbit coupling

have been determined. $PbNbS_2$ with such high superconducting T_c in comparison to other pristine TMD systems, provides a platform to investigate interesting physics.

3.2 Experimental details

Polycrystalline samples of $PbNbS_2$ were synthesized by the solid state reaction of elemental Pb with NbS_2. The phase purity of the sample was verified by the powder X-ray diffraction using a Bruker D8 advance diffractometer with Cu-Kα radiation. A conventional four probe technique was used for the transport property measurements, carried out in a liquid helium cryostat equipped with a superconducting vector magnet. Field dependent as well as temperature dependent magnetization studies were carried out using a Superconducting Quantum Interference Device (SQUID, Quantum Design). The specific heat data were taken by the time relaxation technique using a Physical Property Measurement System (PPMS, Quantum Design). Detail experimental procedure is discussed in Chapter 2.

3.3 Results and discussion

3.3.1 Structural properties

Rietveld fit for the room temperature powder X-ray diffraction pattern of polycrystalline $PbNbS_2$ has been shown in Fig. 3.1(a). A shifted Chebyschev polynomial of first kind with 10 variables was used for background modelling and the shape of peaks were described by Thompson-Cox-Hastings pseudo-Voigt function. The reliability factor of $R_{wp} = 5.13\%$ with a goodness of fit $\chi^2 = 1.48\%$ demonstrate a reasonably good fitting. $PbNbS_2$ crystallizes in a centrosymmetric hexagonal structure with $P6_3/mmc$ space group. Lattice parameters $a = 3.310(2)$ Å and $c = 11.891(1)$ Å for 2H-NbS_2 become $a = 3.3334(7)$ Å and $c = 17.580(4)$ Å due to intercalation effect, suggests successful insertion of Pb into the van der Waals (vdW) layers of NbS_2.

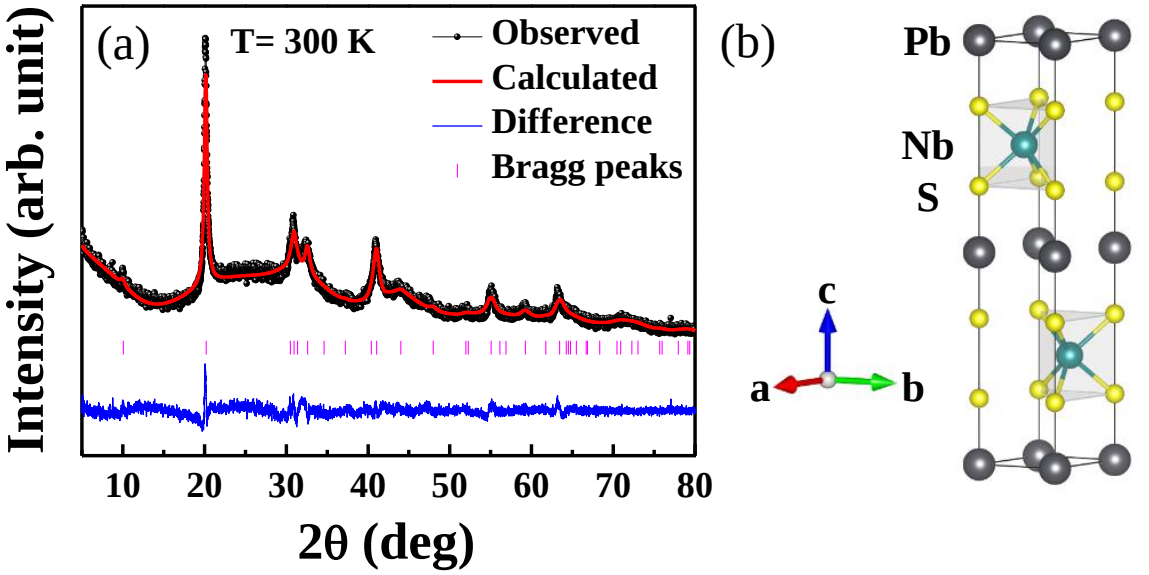

Figure 3.1. (a) Rietveld fitted room temperature powder X-ray diffraction pattern of polycrystalline $PbNbS_2$. Vertical bars indicate the allowed Bragg's reflections for hexagonal $P6_3/mmc$ phase. Blue line indicates the difference between observed and fitted patterns. (b) Crystal structure of $PbNbS_2$.

Fig. 3.1(b) shows crystal structure of $PbNbS_2$ consisting alternative NbS_2 and Pb layers. In the layered structure, Nb accommodates in the trigonal-prismatic coordination with Se atoms whereas Pb occupies the octahedral site. The inversion symmetry as well as two-fold screw rotational symmetry in NbS_2 gets preserved after the intercalation of Pb.

3.3.2 Transport properties

Resistivity of polycrystalline $PbNbS_2$ has been studied as a function of temperature from 2 K to 300 K as shown in the Fig. 3.2(a). The normal state resistivity reveals a metallic nature ($d\rho/dT > 0$) with residual resistivity ratio RRR = $\rho_{300K}/\rho_{9K} = 4.69$. Linear characteristic of the high temperature resistivity, as shown by the solid red line, suggests dominance of electron-phonon scattering. Enlarged view of resistivity data at the low temperature region has been depicted in Fig. 3.2(b). A sharp superconducting transition is observed with critical temperature $T_c^{onset} \sim 8.8$ K and transition width $\Delta T_c \sim 1$ K. Temperature dependence of resistivity data in the range of 9 – 50 K

has been fitted to power law $\rho = \rho_0 + AT^2$ as shown by the solid green line in Fig. 3.2(a). The T^2 dependence of resistivity in the temperature range indicates Fermi liquid behaviour of the system. Fitting yields the residual resistivity $\rho_0 = 5.3$ $\mu\Omega$ cm and coefficient $A = 0.0006$ $\mu\Omega$ cm/K^2. The value of ρ_0 is quite small, indicates highly conducting nature of the sample.

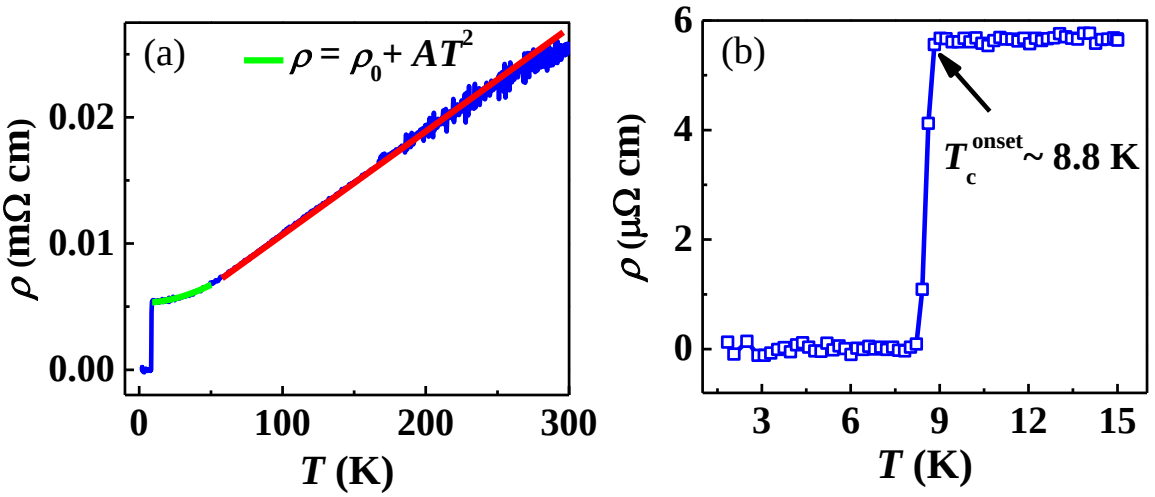

Figure 3.2. (a) Temperature dependent resistivity of $PbNbS_2$. The solid red line is a guide to the linear behaviour of the resistivity in the high temperature range. The solid green line represents the $\rho = \rho_0 + AT^2$ fit. (b) Enlarged view of ρ vs. T data at low temperature showing the superconducting transition.

Temperature dependence of resistivity has been studied at various applied magnetic fields in the temperature range of 2 – 11 K as depicted in Fig. 3.3(a). A variable magnetic field of 0 – 1 T was applied perpendicular to the probe current. Finding the T_c at different magnetic fields, the upper critical field values H_{c2} have been plotted as a function of temperature as shown in Fig. 3.3(b). The temperature dependence of H_{c2} data has been fitted (solid red line) with generalized Ginzburg-Landau (GL) formula $H_{c2}(T) = H_{c2}(0)(1–t^2)/(1 + t^2)$, where $t = T/T_c$ and T_c is the transition temperature at zero field. The upper critical field at $T = 0$ K determined from the GL fit is $\mu_0 H_{c2}(0) = 1.56$ T. Temperature dependent H_{c2} data has an upward like nature at the low temperature region and therefore deviates from the GL fit. This upward feature indicates possible multiband mechanism that can also be seen for isoelectronic $PbTaSe_2$ [37], $SnTaS_2$ [44] and $PbTaS_2$ [45]. Further,

the $H_{c2}(T)$ data has been fitted (solid blue line) with $H_{c2}(T) = H_{c2}(0)(1–t^{3/2})^{3/2}$ equation [125], where $t = T/T_c$, provides a better fit with $R^2 = 0.99809$. The upper critical field determined from this model is $\mu_0 H_{c2}(0) = 1.88$ T. This model has been earlier used to fit the $H_{c2}(T)$ data for $PbTaSe_2$ [37], $Nb_{0.18}Re_{0.82}$ [126] and borocarbide superconductors [127]. Using $\mu_0 H_{c2}(0) = 1.88$ T for $T = 0$ K, the superconducting coherence length is determined to be $\xi_{GL}(0) = [\Phi_0/2\pi H_{c2}(0)]^{1/2} = 13.2$ nm, where $\Phi_0 = h/2e$.

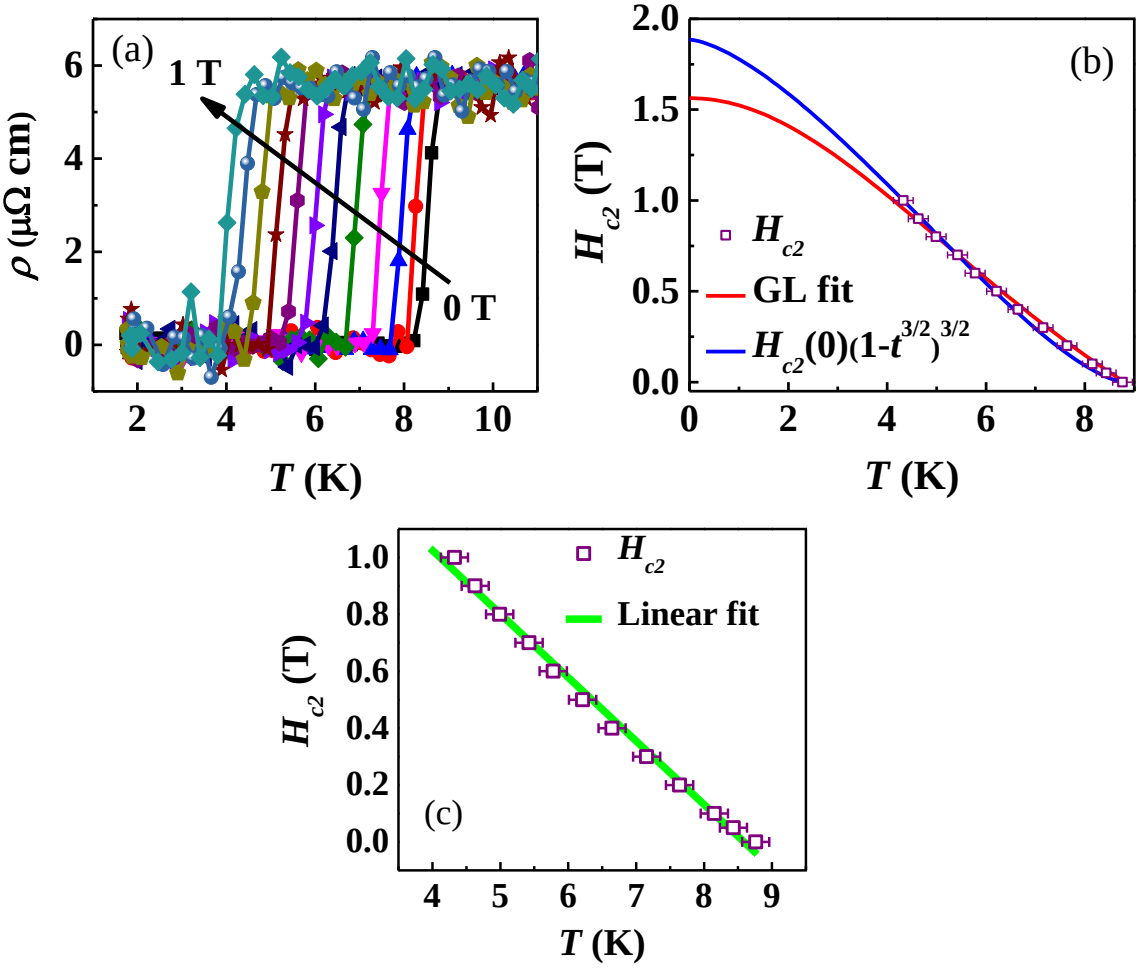

Figure 3.3. (a) Superconducting transition from temperature dependent resistivity under various applied magnetic fields. (b) Temperature dependence of the upper critical field extracted from the resistivity curves. The solid red line represents the Ginzburg-Landau fit and the solid blue line shows the fitting of the upper critical field data to $H_{c2}(T) = H_{c2}(0)(1–t^{3/2})^{3/2}$ equation. (c) Linear fit (solid green line) to the temperature dependence of upper critical field data.

Again, for a single band BCS type superconductor, the orbital upper critical field

can be obtained from Werthamer-Helfand-Hohenberg (WHH) formula $H_{c2}^{orb}(T) = -AT_c(dH_{c2}/dT)_{T=T_c}$ where $A = 0.69$ and 0.72 for the dirty and clean limits respectively [54]. Temperature dependent H_{c2} values have been linearly fitted as shown by the solid green line in the Fig. 3.3(c) and the slope is determined to be $dH_{c2}/dT = -0.22$ T/K. Hence taking $T_c = 8.8$ K the orbital critical field is found to be $H_{c2}^{orb}(T) = 1.33$ T and 1.39 T for the dirty and clean limits respectively. Furthermore, the Pauli limiting upper critical field [55, 56] can be determined from $H_P = \Delta/\sqrt{2}\mu_B$ where $\Delta = 1.76k_BT_c$ and hence found to be $\mu_0 H_P = 16.28$ T. Hence, $H_{c2}^{orb}(T) < H_{c2} < H_P$ which suggests the superconductivity in $PbNbS_2$ to be Pauli limited. The Maki parameter $\alpha = \sqrt{2}H_{c2}^{orb}/H_P$ [128] is determined to be 0.12 is less than 1 and therefore, the Fulde-Ferrell-Larkin-Ovchinnikov (FFLO) state [129, 130] which is reflective of the spatially modulated order parameter is not favourable.

3.3.3 Magnetic properties

Zero field cooled (ZFC) and field cooled (FC) temperature dependent DC magnetic susceptibility of $PbNbS_2$ has been studied from 2 K to 15 K with an applied external magnetic field of 20 Oe as shown in Fig. 3.4(a). Superconductivity has been confirmed from the nature of the diamagnetic signals in both the ZFC and FC curves showing Meissner effect. The smaller FC signal in comparison to the ZFC signal is caused by vortex pinning which is associated with type-II superconductivity. The superconducting transition temperature determined from the susceptibility data is 8.6 K which is in good agreement with that derived from the resistivity study.

Fig. 3.4(b) displays isothermal field dependence of the magnetization of $PbNbS_2$ studied at 6 K. A magnetic hysteresis loop has been observed that confirms type-II superconductivity.

To determine the lower critical field of $PbNbS_2$ we have carried out field dependent magnetization at several temperatures with a zero field cooling protocol. Fig. 3.5(a) shows isothermal magnetization at different temperatures from 2 K to 8 K with $\Delta T =$

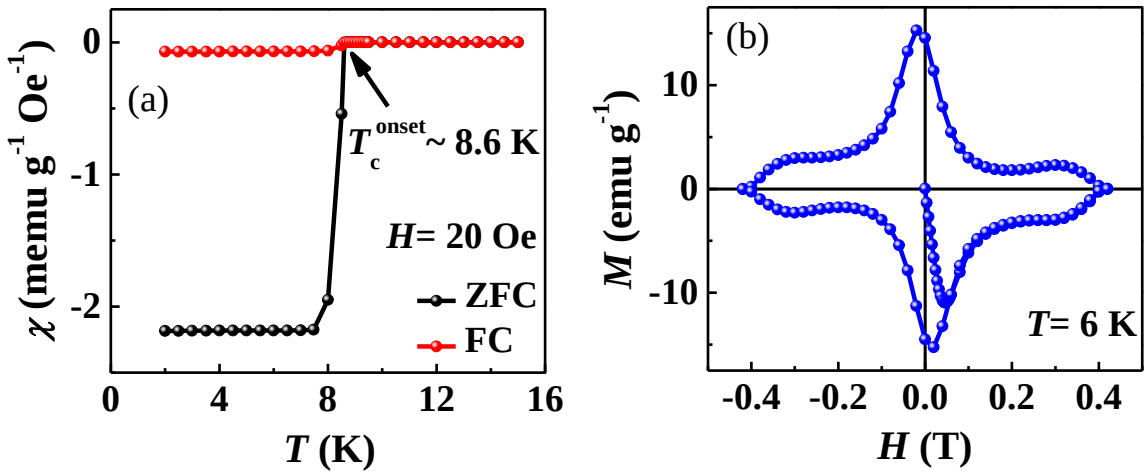

Figure 3.4. (a) Temperature dependent zero field cooled (ZFC) and field cooled (FC) magnetic susceptibility with an applied magnetic field of 20 Oe. (b) Isothermal field dependent magnetization studied at 6 K.

1 K and the solid green line shows the linear fit in the low field range. Magnetization starts to deviate from the linear fit with the increase of the applied magnetic field, giving a lower critical field H_{c1} for each isotherm. These experimental lower critical field values are then fitted with the formula $H_{c1}(T) = H_{c1}(0)(1–t^2)$ where $t = T/T_c$ as shown by the solid red line in the Fig. 3.5(b). From this fit the zero temperature lower critical field is determined to be $\mu_0 H_{c1}(0) = 38.4$ mT.

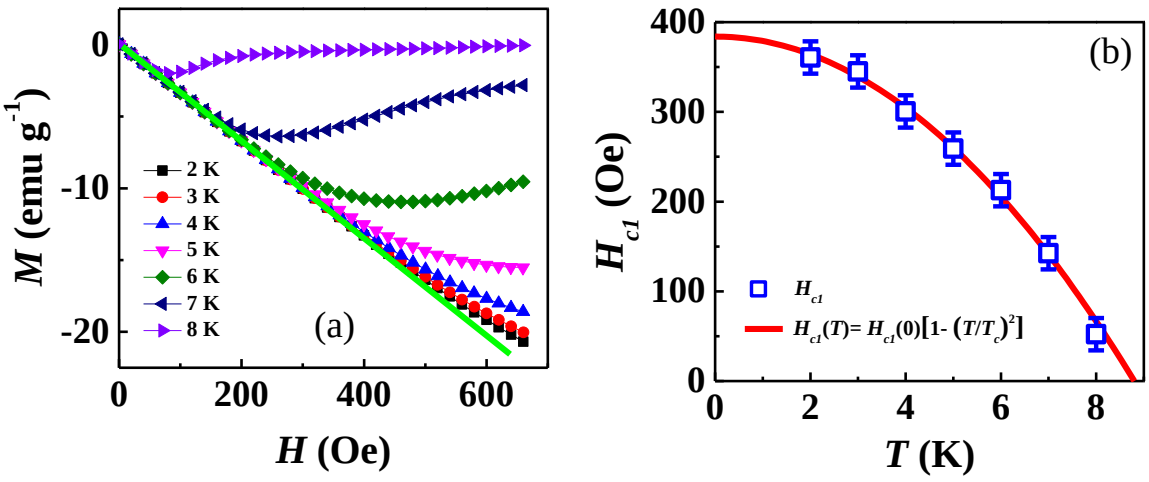

Figure 3.5. (a) Zero field cooled (ZFC) isothermal magnetization at different temperatures. The solid green line is the linear fit to the 2 K data in the low field range. (b) Lower critical field extracted from the isothermal magnetization curves. The solid red line represents the $H_{c1}(T) = H_{c1}(0)[1–(T/T_c)^2]$ fit to the temperature dependence of the lower critical fields.

The Ginzburg-Landau superconducting penetration depth can be calculated from the formula $\mu_0 H_{c1}(0) = (\Phi_0/4\pi\lambda_{GL}^2) ln(\lambda_{GL}/\xi_{GL})$ to give $\lambda_{GL}(0) = 90.94$ nm. Therefore, the Ginzburg-Landau parameter to be determined as $\kappa = \lambda_{GL}(0)/\xi_{GL}(0) = 6.85$ indicating that $PbNbS_2$ is a type-II superconductor. Further, the thermodynamic critical field of $PbNbS_2$ can be determined from the relation $H_{c1}(0)H_{c2}(0) = H_c(0) ln(\kappa)$ and found to be $\mu_0 H_c(0) = 193.7$ mT. The superconducting coherence length of $PbNbS_2$ is smaller and the thermodynamic critical field of $PbNbS_2$ is quite high in comparison to that of noncentrosymmetric $PbTaSe_2$ [37].

3.3.4 Thermodynamic properties

To further investigate the superconductivity in $PbNbS_2$ temperature dependent specific heat measurement has been carried out with applied magnetic fields of H= 0 T and 5 T as depicted in Fig. 3.6(a). At H= 0 T the specific heat data shows a sharp jump demonstrating superconductivity and the transition temperature $T_c \sim 8.4$ K has been determined by the isoentropic method shown in the Fig. 3.6(b). Applying magnetic field of H= 5 T completely suppress the superconducting transition and the C/T vs. T^2 curve can be well fitted by the relation $C/T = \gamma + \beta T^2$ as shown by the solid red line in the Fig. 3.6(c). From the fit we can determine the normal state Sommerfield coefficient $\gamma = 33.08$ mJ mol^{-1} K^{-2} and the phonon-specific coefficient $\beta = 0.42$ mJ mol^{-1} K^{-4}. The $\Delta C/\gamma T_c$ parameter is calculated to be 1.54, which is larger than the theoretical value of 1.43 for a conventional weak coupling BCS superconductor suggests moderately enhanced electron-phonon coupling.

From $\Theta_D = [(12/5\beta)\pi^4 n N_A k_B]^{1/3}$, where n = 4 for $PbNbS_2$, N_A is the Avogadro number and k_B is Boltzmann's constant, the characteristic Debye temperature is estimated to be $\Theta_D = 263.9$ K. The electron-phonon coupling constant λ_{ep} can be determined using the McMillan's formula [131], $\lambda_{ep} = [1.04 + \mu^* ln(\Theta_D/1.45T_c)]/[(1–0.62\mu^*) ln(\Theta_D/1.45T_c)–1.04]$. Taking $\mu^* = 0.13$ the value of λ_{ep} is found to be 0.81 which is lesser than 1, the minimum value for a strong

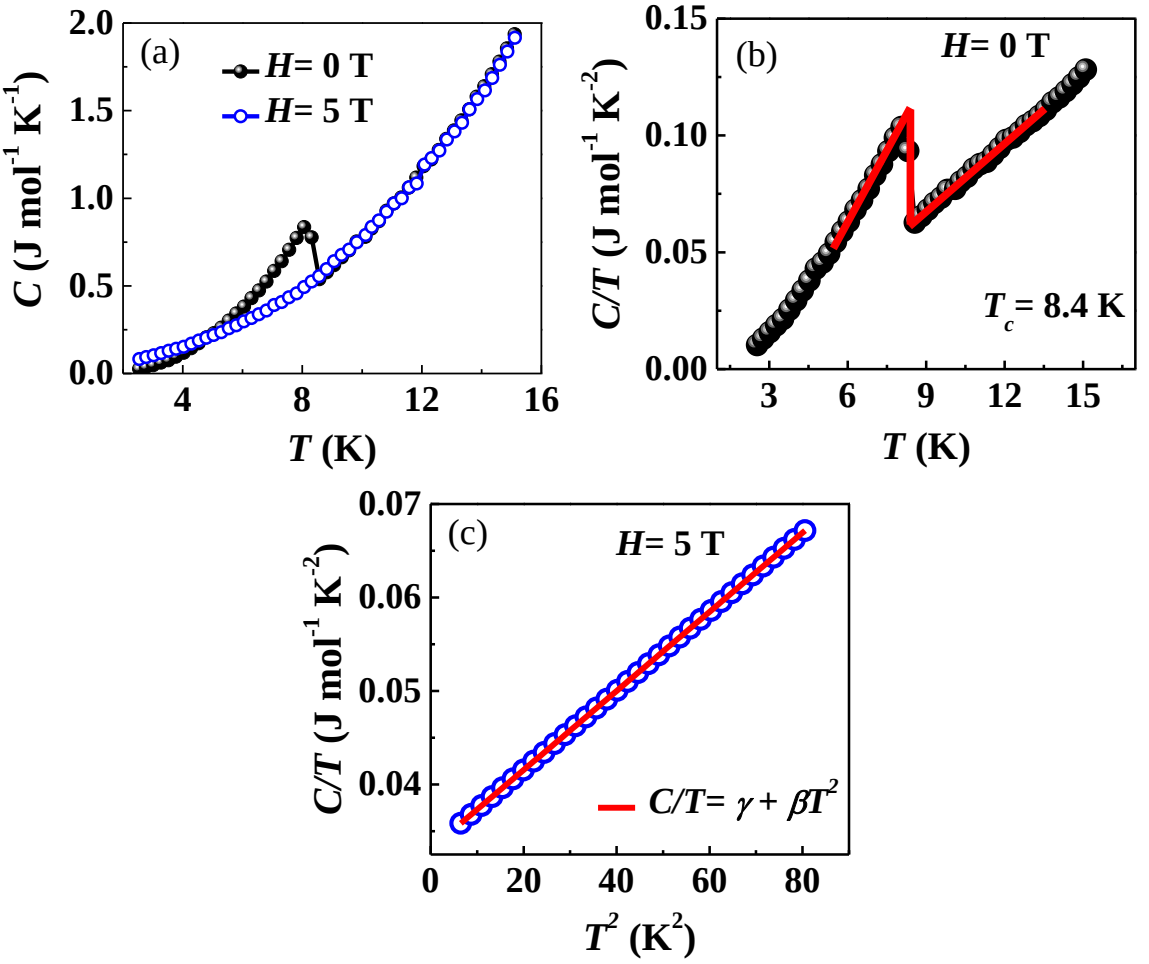

Figure 3.6. (a) Temperature dependent specific heat measured at $H = 0$ T and 5 T. (b) C/T vs. T data at $H = 0$ T showing the bulk superconducting jump and the isoentropic approach for T_c determination. (c) Low temperature C/T vs. T^2 data for $H = 5$ T fitted with $C/T = \gamma + \beta T^2 + \delta T^4$ equation.

coupling, suggests $PbNbS_2$ is a moderately coupled superconductor. Using these results one can derive the noninteracting density of states at Fermi level from $N(E_F) = 3\gamma/[\pi^2 k_B^2(1 + \lambda_{ep})]$, gives $N(E_F) = 7.77$ states eV^{-1} per formula unit. The value of Debye temperature Θ_D, electron-phonon coupling constant λ_{ep} and density of states at Fermi level $N(E_F)$ are comparatively higher than that of the related $PbTaSe_2$ [37] and $SnTaS_2$ [44] systems.

3.4 Conclusions

This chapter introduces $PbNbS_2$ as a transition metal dichalcogenide based layered superconductor with superconducting $T_c \sim 8.8$ K. Synthesis, crystal structure, electrical transport, magnetization and specific heat measurements have been discussed to investigate the physical properties of this system. $PbNbS_2$ crystallizes in a centrosymmetric hexagonal layered structure with $P6_3/mmc$ space group. The layered structure consists of alternative Pb and NbS_2 layers stabilized due to weak van der Waals interaction. Resistivity, magnetic susceptibility and specific heat measurements confirm type-II bulk superconductivity in this system. The superconducting upper and lower critical fields are found to be $\mu_0 H_{c2}(0) = 1.88$ T and $\mu_0 H_{c1}(0) = 38.4$ mT, respectively. The characteristic coherence length and penetration depth are determined to be $\xi_{GL}(0) = 13.2$ nm and $\lambda_{GL}(0) = 90.94$ nm, respectively, with the Ginzburg-Landau parameter value $\kappa(0) = 6.89$. The characteristic Debye temperature determined from the specific heat data to be $\Theta_D = 263.9$ K, while the electron phonon coupling constant $\lambda_{ep} = 0.81$ and $\Delta C/\gamma T_c = 1.54$ signify that $PbNbS_2$ is a moderately coupled superconductor.

Chapter 4

Superconductivity and ferromagnetism in $PbNbSe_2$

4.1 Introduction

The highest superconducting T_c among the pristine transition metal dichalcogenide systems is observed in 2H-$NbSe_2$. $NbSe_2$ is a superconductor below $T_c \sim 7.2$ K, while an incommensurate CDW with $T_{CDW} \sim 35$ K is found to coexist with this highly anisotropic superconductivity [68, 76, 78, 80, 81, 86, 89–106]. The quasi-2D structure consists layers of $NbSe_2$ units, in which Nb atoms are in trigonal prismatic coordination with Se atoms (Fig. 1.5). These layers are strongly bound in the *ab*-plane, while a weak van der Waals force stabilizes these layers along the *c*-axis. Introduction of intercalants, even in small amount, into these layers can significantly affect the crystal structure and the physical properties of this system.

We have prepared polycrystalline samples of $PbNbSe_2$. Pb intercalation in $NbSe_2$ layers has been realized via solid state reaction method. Detail structural, transport and magnetic properties studies have been carried out. $PbNbSe_2$ is found to be superconducting with $T_c \sim 5.75$ K. A weak ferromagnetic feature is observed to emerge in the close vicinity of superconductivity with $T_{FM} \sim 4.4$ K, indicates coexistence of superconductivity and ferromagnetism in $PbNbSe_2$. Concurrence of

two mutually exclusive phenomena, superconductivity and ferromagnetism, is a novel characteristic of this system.

4.2 Experimental details

Polycrystalline $PbNbSe_2$ samples were synthesized via solid state reaction route taking Pb, Nb and Se in elemental form. The phase purity of the sample was verified by the powder X-ray diffraction using a Bruker D8 advance diffractometer with Cu-Kα radiation. A standard four probe technique was used for the transport property measurements, carried out in a liquid helium cryostat equipped with a superconducting vector magnet. Field dependent as well as temperature dependent magnetization studies were carried out using a Superconducting Quantum Interference Device (SQUID, Quantum Design). Detailed experimental procedure is discussed in Chapter 2.

4.3 Results and discussion

4.3.1 Structural properties

The room temperature powder X-ray diffraction pattern of polycrystalline $PbNbSe_2$ has been fitted with Rietveld method as shown in Fig. 4.1(a). Background was modelled using a shifted Chebyschev polynomial of the first kind with 10 variables and peak shapes were described by Thompson-Cox-Hastings pseudo-Voigt function. The reliability factor $R_{wp} = 7.69\%$ and the goodness of fit $\chi^2 = 2.06\%$ indicate a reasonably good fit. $PbNbSe_2$ crystallizes in a centrosymmetric hexagonal structure with $P6_3/mmc$ space group. Significant change in lattice parameters from $a = 3.444(1)$ Å and $c = 12.544(2)$ Å for 2H-$NbSe_2$ to $a = 3.4344(2)$ Å and $c = 18.523(1)$ Å for $PbNbSe_2$ implies a successful intercalation of Pb into the van der Waals (vdW) layers of $NbSe_2$.

Crystal structure of $PbNbSe_2$ has been depicted in Fig. 4.1(b). The layered

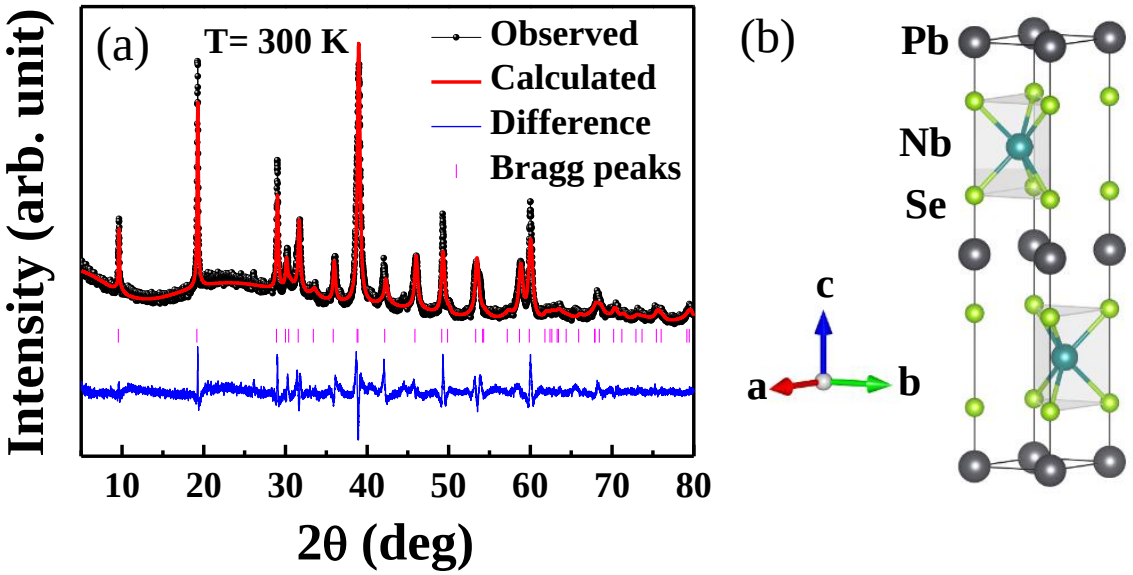

Figure 4.1. (a) Rietveld fitted room temperature powder X-ray diffraction pattern of polycrystalline $PbNbSe_2$. Vertical bars indicate the allowed Bragg's reflections for hexagonal $P6_3/mmc$ phase. Blue line indicates the difference between observed and fitted patterns. (b) Crystal structure of $PbNbSe_2$.

structure consists of alternative $NbSe_2$ and Pb layers. Nb is in trigonal-prismatic co-ordination by the Se atoms whereas Pb occupies the octahedral co-ordination. $PbNbSe_2$ preserves the inversion as well as the two-fold screw rotational symmetries of hexagonal 2H-$NbSe_2$.

4.3.2 Transport properties

Temperature dependence of resistivity of polycrystalline $PbNbSe_2$ in the temperature range of 2 – 300 K is shown in Fig. 4.2(a). The normal state resistivity shows a metallic nature ($d\rho/dT > 0$) with residual resistivity ratio RRR = ρ_{300K}/ρ_{7K} = 2.83. Linear temperature dependence of the resistivity at the high temperature region, as shown by the solid red line, suggests the dominance of electron-phonon scattering. Fig. 4.2(b) shows extended view of resistivity at the low temperature region exhibiting superconducting nature of the sample. Slope of the temperature dependent resistivity data starts to change at $T_c^{onset} \sim 6.5$ K and the zero resistivity is found to be achieved at $T_c^{zero} \sim 4.7$ K. The criterion for selecting the superconducting

transition temperature $T_c \sim 5.75$ K has been demonstrated by the solid black lines. Superconducting T_c has been considered at the intersection of the extrapolations of the steepest slope of the superconducting transition region and the normal state resistivity. Low temperature resistivity data in the range of 7 – 25 K has been fitted (solid green line) to power law $\rho = \rho_0 + AT^2$ and shown in the Fig. 4.2(c). The T^2 dependence of resistivity over this temperature range suggests Fermi liquid behaviour of the system. The residual resistivity is found to be $\rho_0 = 252$ $\mu\Omega$ cm and the coefficient $A = 43$ $\mu\Omega$ cm/K^2. The value of ρ_0 is quite large, most likely due to polycrystalline nature of the sample.

Fig. 4.3(a) depicts the magnetotransport study in the temperature range of 2 – 10 K with applied magnetic field varying from 0 T to 1 T. Field dependence of resistive T_c has been determined and hence upper critical field H_{c2} as a function of temperature is plotted as shown in the Fig. 4.3(b). The temperature dependence of H_{c2} data has been fitted (solid red line) with generalized Ginzburg-Landau (GL) equation $H_{c2}(T) = H_{c2}(0)(1–t^2)/(1+t^2)$, where $t = T/T_c$ and T_c is the transition temperature at zero field. The upper critical field from GL fit is determined to be $\mu_0 H_{c2}(0) =$ 1.84 T. Temperature dependent H_{c2} data has an upward feature and hence deviates from the GL equation at low temperature. This upward curvature possibly arises due to multiband mechanism. Similar upward feature in $H_{c2}(T)$ data is also evident for $PbNbS_2$ (Chapter 3), $SnTaS_2$ [44], $PbTaSe_2$ [37] and $PbTaS_2$ [45]. Therefore, the $H_{c2}(T)$ data has been fitted (solid blue line) with $H_{c2}(T) = H_{c2}(0)(1–t^{3/2})^{3/2}$ equation [125] with $t = T/T_c$, provides a better fit with $R^2 = 0.99819$. The upper critical field is determined to be $\mu_0 H_{c2}(0) = 2.26$ T. This model has been previously used to fit the $H_{c2}(T)$ data for $PbTaSe_2$ [37], $Nb_{0.18}Re_{0.82}$ [126] and borocarbide superconductors [127]. Based on Ginzburg-Landau theory, the superconducting coherence length is given by $\xi_{GL}(0) = [\Phi_0/2\pi H_{c2}(0)]^{1/2}$ where $\Phi_0 = h/2e$. Using the upper critical field $\mu_0 H_{c2}(0) = 2.26$ T, the coherence length is calculated to be $\xi_{GL}(0) = 12.1$ nm.

Alternatively, for a single band, BCS type superconductor, the orbital upper

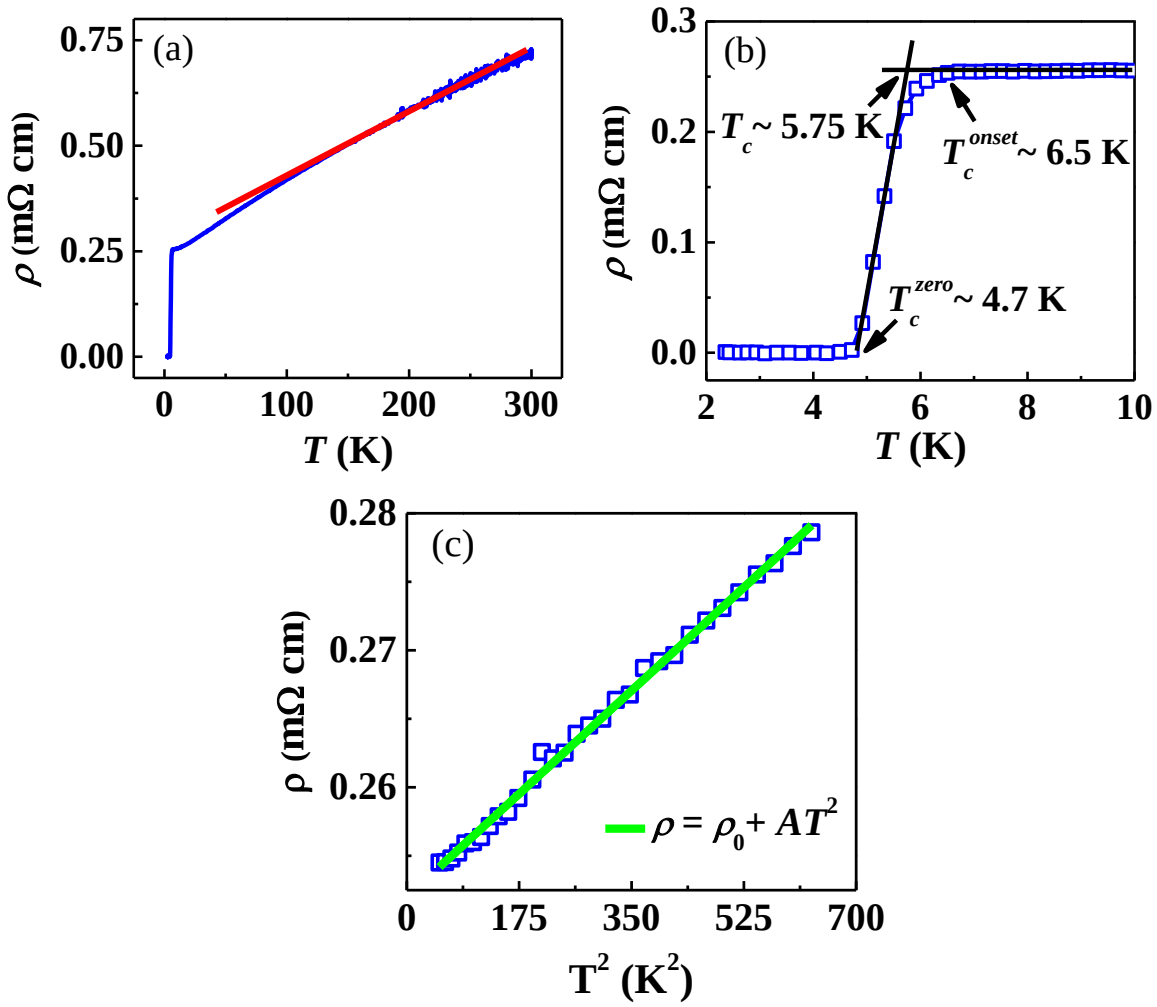

Figure 4.2. (a) Temperature dependent resistivity of $PbNbSe_2$. The solid red line is a guide to the linear behaviour of the resistivity in the high temperature range. (b) Enlarged view of ρ vs. T data at low temperature showing the superconducting transition. (c) Normal state ρ vs. T^2 data at low temperature region fitted (solid green line) with $\rho = \rho_0 + AT^2$ equation.

critical field can be determined using Werthamer-Helfand-Hohenberg (WHH) formula $H_{c2}^{orb}(T) = -AT_c(dH_{c2}/dT)_{T=T_c}$ where A= 0.69 and 0.72 respectively for dirty and clean limits [54]. From the linear fit of the temperature dependent H_{c2} data as shown in the Fig. 4.3(c), slope $dH_{c2}/dT = -$ 0.39 T/K and hence taking T_c = 5.75 K the orbital critical field is found to be $H_{c2}^{orb}(T)$ = 1.56 T and 1.63 T for the dirty and clean limits respectively. Further, the Pauli critical field [55, 56] can be determined from $H_P = \Delta/\sqrt{2}\mu_B$ where $\Delta = 1.76k_BT_c$ and is estimated to be $\mu_0 H_P$ = 10.64 T. Since $H_{c2}^{orb}(T) < H_{c2} < H_P$, the superconductivity in $PbNbSe_2$ is Pauli limited. The

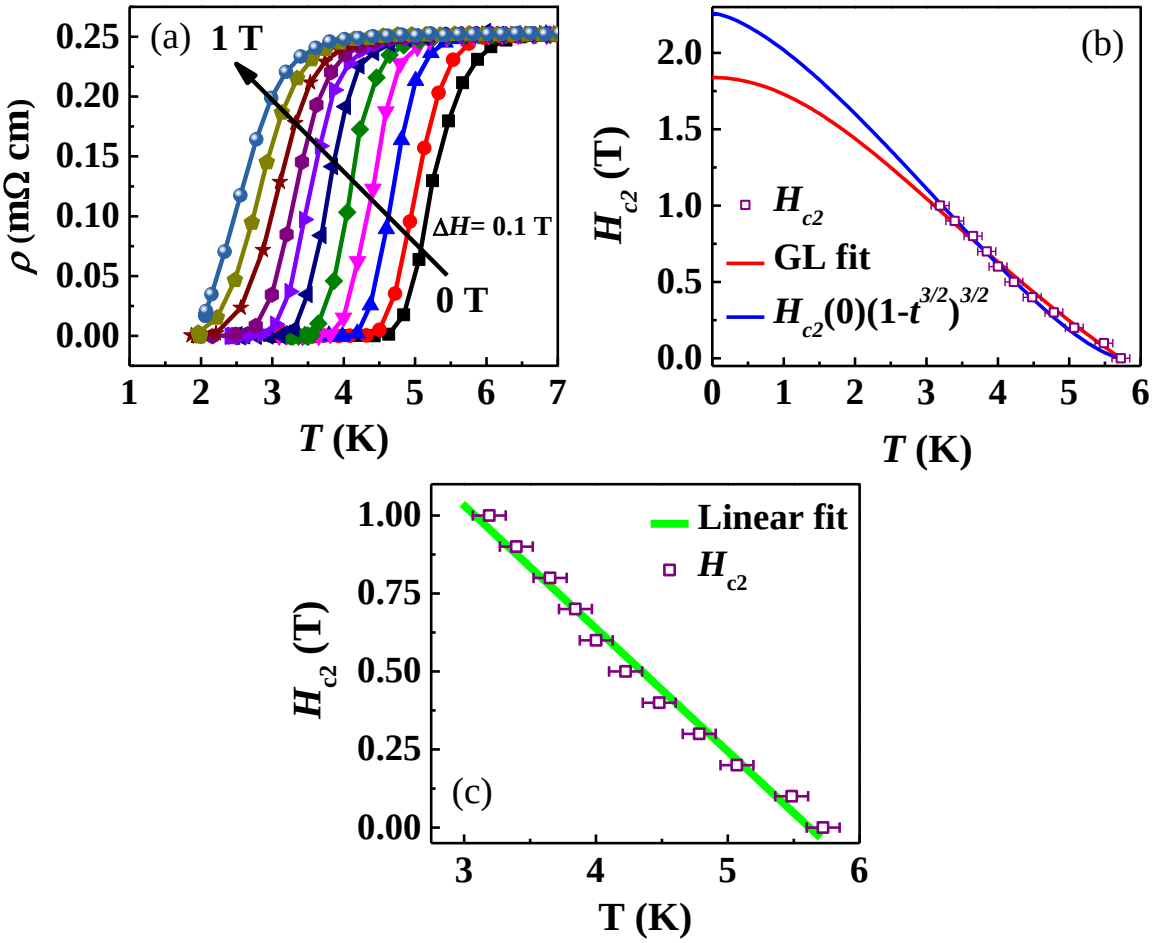

Figure 4.3. (a) Superconducting transition from temperature dependent resistivity under various applied magnetic fields. (b) Temperature dependence of the upper critical field extracted from the resistivity curves. The solid red line represtents the Ginzburg-Landau fit and the solid blue line shows the fitting of the upper critical field data to $H_{c2}(T) = H_{c2}(0)(1–t^{3/2})^{3/2}$ equation. (c) Linear fit (solid green line) to the temperature dependence of upper critical field data.

estimated Maki parameter $\alpha = \sqrt{2}H_{c2}^{orb}/H_P = 0.22$ [128] is less than 1 and hence the Fulde-Ferrell-Larkin-Ovchinnikov (FFLO) state [129, 130], which is reflective of spatially modulated order parameter, is not favourable.

4.3.3 Magnetic properties

Zero field cooled (ZFC) and field cooled (FC) temperature dependent DC magnetic susceptibility of $PbNbSe_2$ has been studied from 2 K to 300 K with applied magnetic field of 20 Oe and 100 Oe as shown in Fig. 4.4(a) and Fig. 4.4(b) respectively.

Superconductivity is further confirmed from the diamagnetic signals in both the 20 Oe and 100 Oe data demonstrating Meissner effect. Fig. 4.4(c) and Fig. 4.4(d) show the enlarged view of the low temperature susceptibility data. The diamagnetic ZFC data in both the cases show a broad superconducting transition similar to the resistivity data. The diamagnetic FC signal at 20 Oe shows a magnetic anomaly and gradually starts increasing below 4.2 K that eventually becomes positive around 3.8 K and then shows a magnetic saturation in the lower temperature range. The nature of the FC curve suggests ferromagnetic ordering below the superconducting transition. The ferromagnetic transition temperature T_{FM} = 4.4 K has been determined from the $d\chi/dT$ vs. T curve as shown in Fig. 4.4(e). Ferromagnetism in the close vicinity of superconductivity is also confirmed from the FC signal of 100 Oe susceptibility data. The FC diamagnetic signal in this case starts to deviate from its usual path and shows a saturation like nature below 4.2 K but never becomes positive as in the case of 20 Oe data. The ferromagnetic transition temperature T_{FM} = 4.4 K, in this case, is further confirmed from the $d\chi/dT$ vs. T curve as shown in Fig. 4.4(f).

Despite the same ferromagnetic transition temperature in both the 20 Oe and 100 Oe cases the nature of the FC curves is quite different. It suggests competitive behaviour between the coexisting superconductivity and the ferromagnetism. At low field (H = 20 Oe) the ferromagnetic ordering becomes dominating below T_{FM} and hence, gives rise to a positive FC signal in the low temperature range. Whereas, in higher magnetic field (H = 100 Oe), the superconducting signal becomes stronger than that of the ferromagnetic signal and gives rise to a saturation like nature in the FC curve while keeping the magnetization negative. This close interaction between superconductivity and ferromagnetism is comparable with the cases for $EuFe_2(As_{0.7}P_{0.3})_2$ [132] and $EuFe_2(As_{1-x}P_x)_2$ [133] where $T_{FM} < T_c$.

To further probe the interplay between superconductivity and ferromagnetism in $PbNbSe_2$, isothermal field dependent magnetization has been studied at 2 K as shown in Fig. 4.5(a). We found a type-II superconducting hysteresis loop to be superimposed with the ferromagnetic signal demonstrating the coexistence

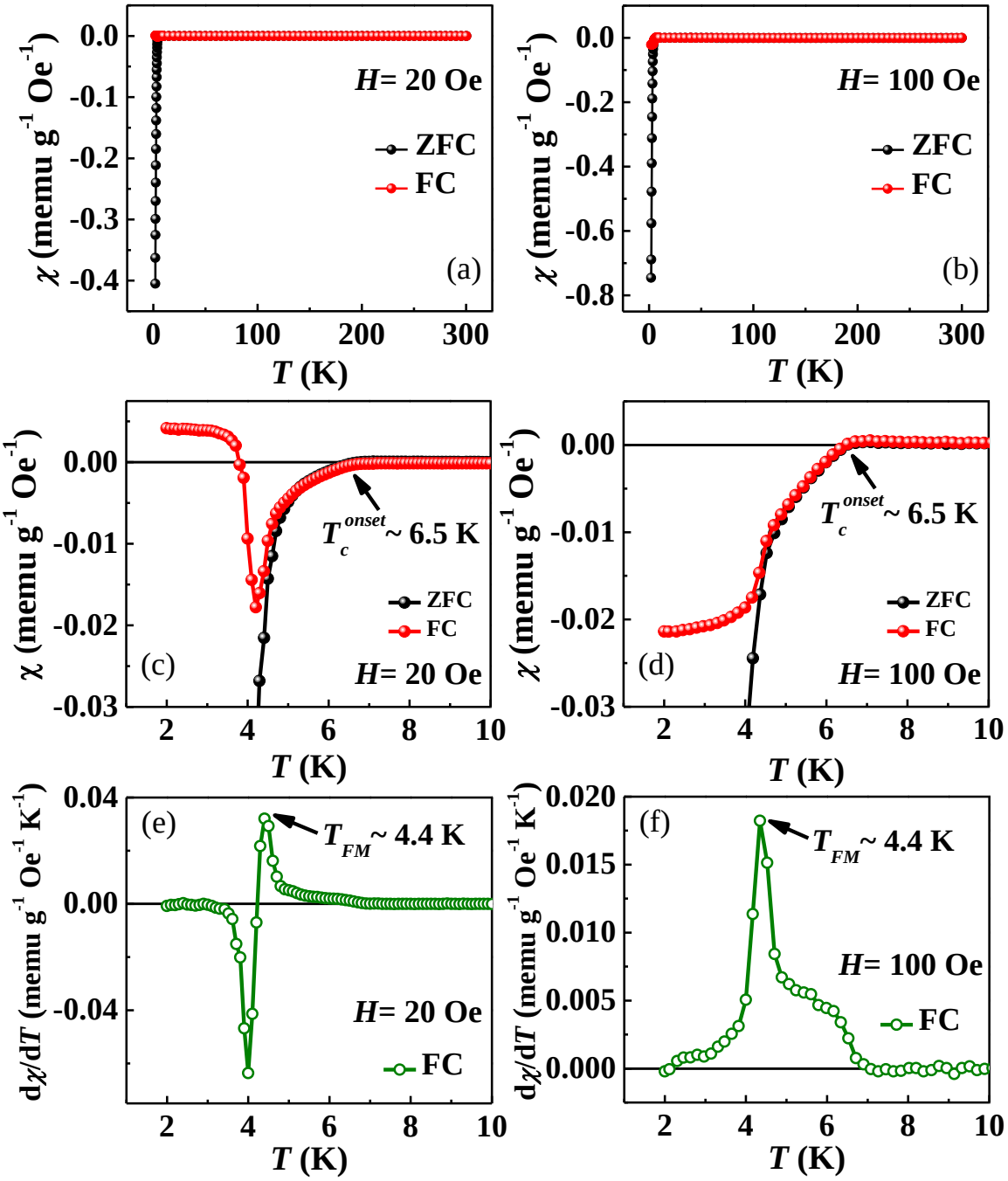

Figure 4.4. Temperature dependent zero field cooled (ZFC) and field cooled (FC) magnetic susceptibility with an applied magnetic field of (a) $H = 20$ Oe and (b) $H = 100$ Oe. (c) and (d) show the extended view of the low temperature susceptibility data. (e) and (f) represent $d\chi/dT$ vs. T curves for $H = 20$ Oe and $H = 100$ Oe data respectively.

of both the phenomena. Similar type of unusual hysteresis loop corresponding to the coexisting superconductivity and ferromagnetism can be observed for $[(Li_{1-x}Fe_x)OH](Fe_{1-y}Li_y)Se$ [134], $EuFe_2(As_{1-x}P_x)_2$ [133], RhGe [135] and surface

modulated 2D-$NbSe_2$ [136]. Fig. 4.5(b) shows the initial diamagnetic curve of the field dependent magnetization and the lower critical field is determined from the deviation of the isotherm from the linear fit (solid green line) to be H_{c1} = 6 Oe at T = 2 K. This diamagnetic signal eventually transforms into a ferromagnetic one with the increasing applied magnetic field as shown in the Fig. 4.5(c).

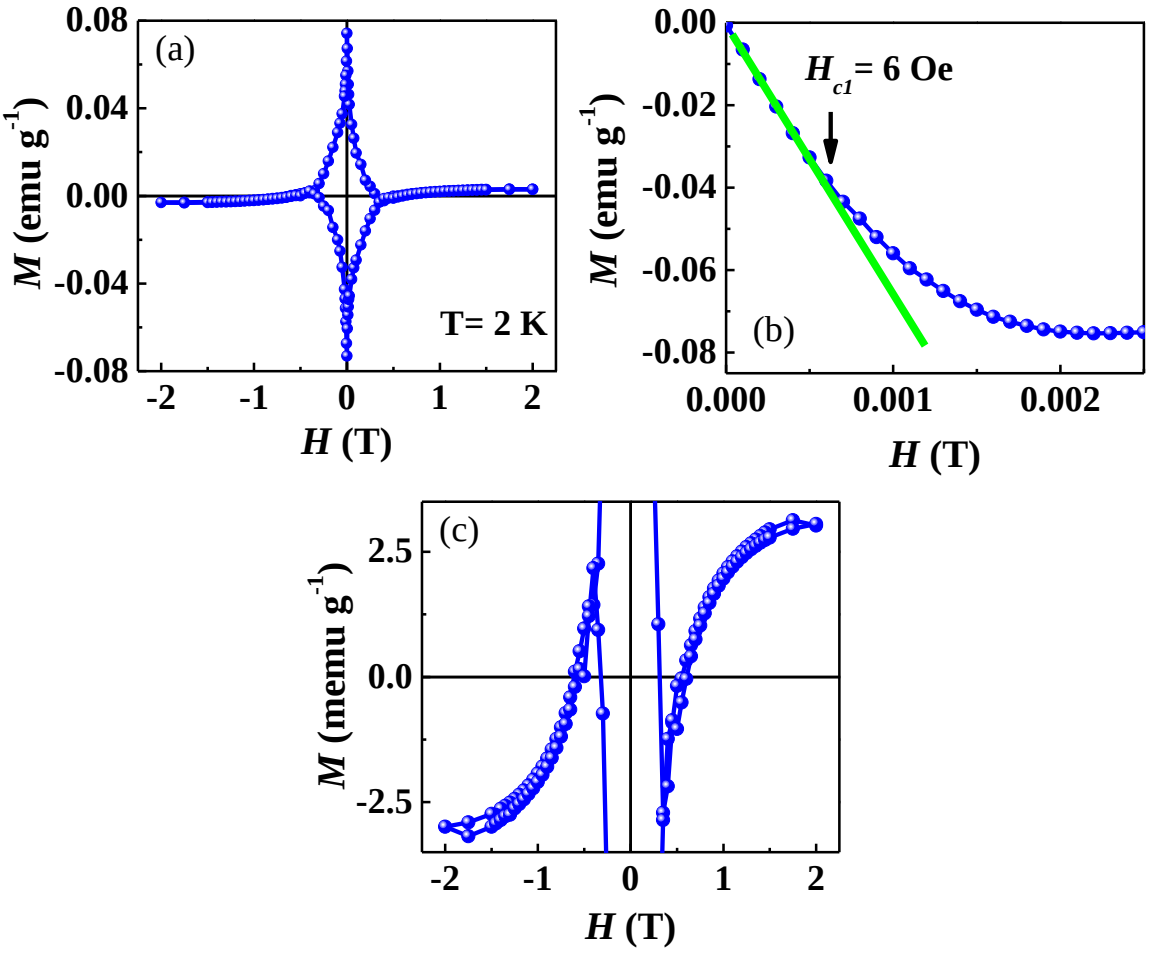

Figure 4.5. (a) Isothermal field dependent magnetization studied at 2 K. (b) Initial diamagnetic curve of the field dependent magnetization. The lower critical field value at T = 2 K has been marked by a down arrow. (c) Extended view of the M vs. H curve.

The ferromagnetism in superconducting $PbNbSe_2$ is comparable with the case of ferromagnetism induced by the surface molecular adsorption in 2D-$NbSe_2$ [136]. Structural modulation occurs due to Pb intercalation in $NbSe_2$ layers results in a longer Nb-Se bond. This bond elongation weakens the covalent Nb-Se interaction and reduces the hybridization of Nb with Se atom, thereby results in accumulation

of unpaired electrons around Nb and hence to ferromagnetism.

4.4 Conclusions

We have synthesized Pb intercalated transition metal dichalcogenide based layered superconductor $PbNbSe_2$ with $T_c \sim 5.75$ K. Synthesis, crystal structure, electrical transport and magnetizatic measurements have been discussed to give insights of the physical properties of this system. $PbNbSe_2$ crystallizes in a centrosymmetric hexagonal layered structure with $P6_3/mmc$ space group. The layered structure containing alternative Pb and $NbSe_2$ layers are stabilized due to weak van der Waals interaction. Resistivity, magnetic susceptibility measurements confirm type-II bulk superconductivity in this system. The superconducting upper critical field is found to be $\mu_0 H_{c2}(0) = 2.26$ T, while the characteristic coherence length is determined to be $\xi_{GL}(0) = 12.1$ nm. Evolution of a weak ferromagnetic ordering is evident in the close vicitity of the superconducting T_c, with $T_{FM} \sim 4.4$ K. Competetive nature of the coexisting superconductivity and ferromagnetism has further been characterized from the isothermal field dependent magnetization, where a superconducting type-II hysteresis loop is found to be superimposed with a ferromagnetic hysteresis loop.

Chapter 5

Superconductivity in $SnTaS_2$

5.1 Introduction

The sub-Kelvin superconductivity in 2H-TaS_2 ($T_c \sim 0.8$ K) [36, 74] can be effectively tuned via intercalation approach as we have discussed in Chapter 1. Superconductivity in this quasi-2D system is associated with CDW phase with $T_{CDW} \sim 78$ K. This hexagonal polytype consists layers of TaS_2 units in which Ta atoms occupy the octahedral position and oriented in a trigonal prismatic coordination with S atoms (Fig. 1.5). These layers are strongly connected via covalent bonding along the *ab*-plane, whereas the bonding along the *c*-axis is quite infirm due to the weak van der Waals interaction.

We have prepared polycrystalline samples of $SnTaS_2$ by solid state reactions and detail structural, transport and magnetic studies have been carried out. We found $SnTaS_2$ to be superconducting with $T_c \sim 2.8$ K. Though the superconductivity in $SnTaS_2$ system was known from 1973 [111] and the corresponding specific heat was measured by Dijkstra *et.al.* [112], detail study of the superconducting properties was still lacking. When we were working on our polycrystalline sample of $SnTaS_2$, a report comes on single crystal of $SnTaS_2$ [44] focussing its superconducting and topological properties. Therefore, it will be of interest to see the variation in the several superconducting parameters in our polycrystalline sample and to compare

them with the reported single crystal system.

5.2 Experimental details

Polycrystalline samples of $SnTaS_2$ were synthesized via solid state reaction route taking elemental Sn and presynthesized TaS_2 in stoicheometric ratio. The phase purity of the sample was verified by the powder X-ray diffraction using a Bruker D8 advance diffractometer with Cu-Kα radiation. A standard four probe technique was used for the transport property measurements, carried out in a liquid helium cryostat equipped with a superconducting vector magnet. Field dependent as well as temperature dependent magnetization studies were carried out using a Superconducting Quantum Interference Device (SQUID, Quantum Design) and a Physical Properties Measurement System (PPMS, Quantum Design). Detail experimental procedure is discussed in Chapter 2.

5.3 Results and discussion

5.3.1 Structural properties

Rietveld fit to the room temperature powder X-ray diffraction pattern of polycrystalline $SnTaS_2$ has been demonstrated in Fig. 5.1(a). A shifted Chebyschev polynomial of first kind with 10 variables was used to model the background and the peak shapes were described by Thompson-Cox-Hastings pseudo-Voigt function. Reliability factor of $R_{wp} = 7.20\%$ with a goodness of fit $\chi^2 = 1.69\%$ demonstrate a reasonably good fitting. $SnTaS_2$ crystallizes in a centrosymmetric hexagonal structure with $P6_3/mmc$ space group. The refined lattice parameters are $a = 3.3006(2)$ Å and $c = 17.404(1)$ Å for $SnTaS_2$ shows adequate increase specifically in the c-lattice parameter in comparison to $a = 3.314(2)$ Å and $c = 12.097(1)$ Å for TaS_2. This suggests successful intercalation of Sn atoms in between the van der Waals (vdW) layers of TaS_2.

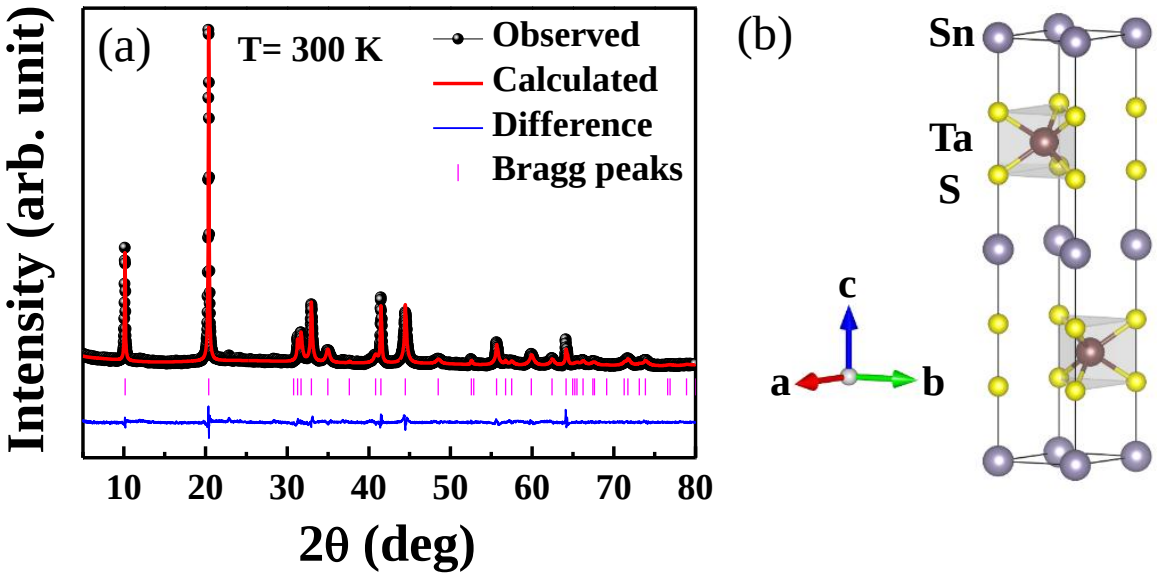

Figure 5.1. (a) Rietveld fitted room temperature powder X-ray diffraction pattern of polycrystalline $SnTaS_2$. Vertical bars indicate the allowed Bragg's reflections for hexagonal $P6_3/mmc$ phase. Blue line indicates the difference between observed and fitted patterns. (b) Crystal structure of $SnTaS_2$.

Fig. 5.1(b) shows the crystal structure of $SnTaS_2$ consist of alternative TaS_2 and Sn layers. In this structure Ta occupies the trigonal-prismatic position coordinated with S atoms and Sn accommodates the octahedral site. The inversion symmetry as well as the two fold screw rotational symmetry in TaS_2 remain unaltered after the intercalation of Sn in the crystal structure.

5.3.2 Transport properties

Temperature dependence of resistivity at zero applied magnetic field has been studied for polycrystalline $SnTaS_2$ from 2 K to 300 K as shown in Fig. 5.2(a). The normal state resistivity shows a metallic behaviour ($d\rho/dT > 0$) with residual resistivity ratio RRR $= \rho_{300K}/\rho_{3K} = 6.78$. Linear nature of the resistivity at high temperature has been shown by the solid red line suggests dominance of electron-phonon scattering. Fig. 5.2(b) shows enlarged view of low temperature resistivity data depicting a sharp superconducting drop with transition temperature $T_c^{onset} \sim 2.8$ K and transition width $\Delta T_c \sim 0.1$ K. Temperature dependent resistivity data in the range of 3 – 60 K has

been fitted with power law $\rho = \rho_0 + AT^2$ as shown by the solid green line in Fig. 5.2(a). The T^2 dependence of resistivity in this temperature range suggests Fermi liquid behaviour of the system. From the fit we found the residual resistivity $\rho_0 = 8.34\ \mu\Omega$ cm and coefficient $A = 0.0024\ \mu\Omega$ cm/K^2. The small value of ρ_0 indicates highly conducting nature of the sample.

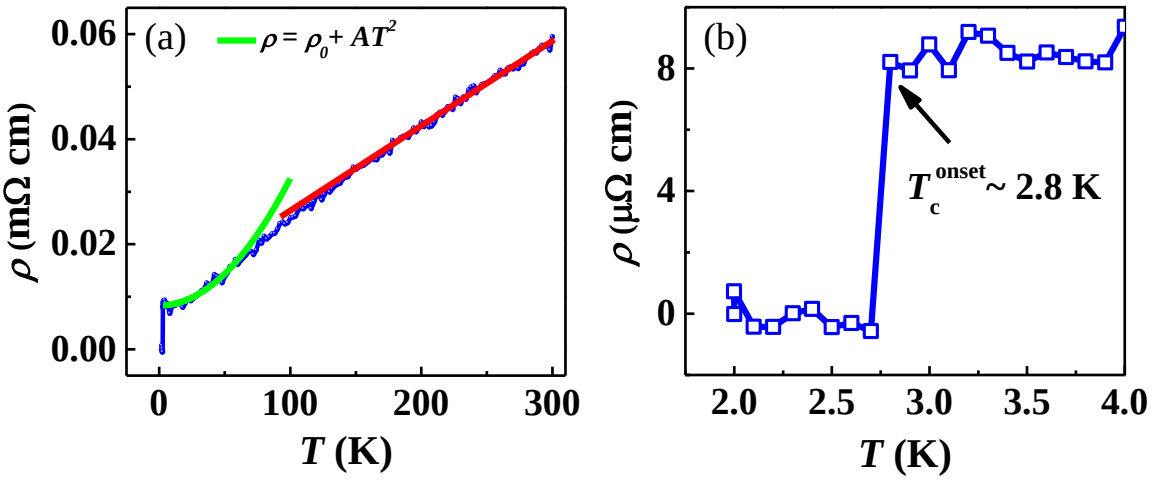

Figure 5.2. (a) Temperature dependent resistivity of $PbNbS_2$. The solid red line is a guide to the linear behaviour of the resistivity in the high temperature range. The solid green line represents the $\rho = \rho_0 + AT^2$ fit. (b) Enlarged view of ρ vs. T data at low temperature showing the superconducting transition.

Temperature dependent resistivity at varying magnetic field has been studied in the temperature range of 2 – 4 K as shown in the Fig. 5.3(a). A variable magnetic field of 0 – 300 Oe was applied perpendicular to the probe current. After finding the T_c as the mid-point of the transition at different magnetic fields, the upper critical field values H_{c2} have been plotted as a function of temperature shown in the main panel of Fig. 5.3(b). The high field temperature dependent H_{c2} data has been fitted (solid red line) with generalized Ginzburg-Landau (GL) formula $H_{c2}(T) = H_{c2}(0)(1–t^2)/(1+t^2)$, where $t = T/T_c$ and T_c is the transition temperature at zero magnetic field. The GL fitting yields the upper critical field at $T = 0$ K to be $\mu_0 H_{c2}(0) = 1170$ Oe. Temperature dependent H_{c2} data has an upward like nature at the low temperature region and therefore considerably deviates from the GL fit. This upward feature arises possibly due to intrinsically anomalous pairing mechanism that can also be

seen for $PbNbS_2$ (Chapter 3), $PbNbSe_2$ (Chapter 4), $PbTaSe_2$ [37], $SnTaS_2$ single crystal [44] and $PbTaS_2$ [45]. Therefore, the H_{c2} data has been further fitted (solid blue line) with $H_{c2}(T) = H_{c2}(0)(1–t^{3/2})^{3/2}$ equation [125] where $t = T/T_c$, provides a better fit with $R^2 = 0.99998$. The upper critical field determined from this model is $\mu_0 H_{c2}(0) = 1458$ Oe. This model has been used earlier for fitting the $H_{c2}(T)$ data of $PbTaSe_2$ [37], $Nb_{0.18}Re_{0.82}$ [126] and borocarbide superconductors [127]. Using $\mu_0 H_{c2}(0) = 1458$ Oe for $T = 0$ K, the superconducting coherence length is determined to be $\xi_{GL}(0) = [\Phi_0/2\pi H_{c2}(0)]^{1/2} = 47.5$ nm, where $\Phi_0 = h/2e$.

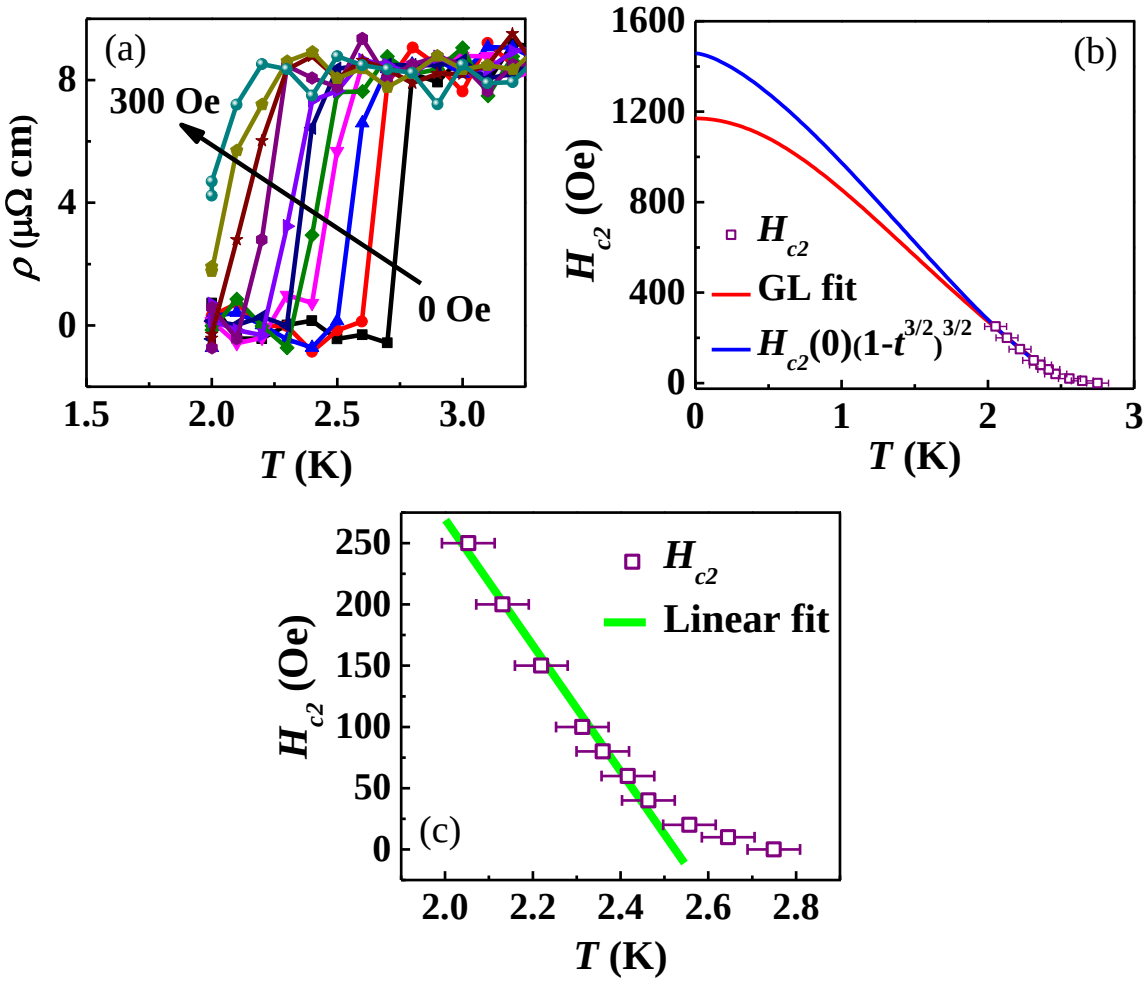

Figure 5.3. (a) Superconducting transition from temperature dependent resistivity under various applied magnetic fields. (b) Temperature dependence of the upper critical field extracted from the resistivity curves. The solid red line represtents the Ginzburg-Landau fit and the solid blue line shows the fitting of the upper critical field data to $H_{c2}(T) = H_{c2}(0)(1–t^{3/2})^{3/2}$ equation. (c) Linear fit (solid green line) to the temperature dependence of upper critical field data.

For a single band BCS type superconductor, the orbital upper critical field can be determined from Werthamer-Helfand-Hohenberg (WHH) formula $H_{c2}^{orb}(T) = -AT_c(dH_{c2}/dT)_{T=T_c}$ where $A = 0.69$ and 0.72 for dirty and clean limits respectively [54]. The linearly best fitted (solid green line) high field temperature dependent H_{c2} values are shown in Fig. 5.3(c) and the slope is determined to be $dH_{c2}/dT = -510$ Oe/K. Hence taking $T_c = 2.75$ K (midpoint of the zero field resistivity transition) the orbital critical field is found to be $H_{c2}^{orb}(T) = 968$ Oe and 1010 Oe for the dirty and clean limits respectively. Further, the Pauli critical field [55, 56] is determined from $H_P = \Delta/\sqrt{2}\mu_B$ where $\Delta = 1.76k_BT_c$ and found to be $\mu_0 H_P = 5.09$ T. Therefore, $H_{c2}^{orb}(T) < H_{c2} < H_P$ which suggests the superconductivity in $SnTaS_2$ is Pauli limited. The Maki parameter $\alpha = \sqrt{2}H_{c2}^{orb}/H_P$ [128] is determined to be 0.02 which is less than 1 and therefore, the Fulde-Ferrell-Larkin-Ovchinnikov (FFLO) state [129, 130] is not favourable.

5.3.3 Magnetic properties

Temperature dependent DC magnetic susceptibility of polycrystalline $SnTaS_2$ has been studied in the temperature range of 2 – 300 K under both the zero field cooled (ZFC) and field cooled (FC) protocols with applied magnetic field of 20 Oe as shown in Fig. 5.4(a). Superconductivity below ~ 3 K has been confirmed from the diamagnetic signals in both the ZFC and FC curves demonstrating characteristic Meissner effect. The smaller diamagnetic signal for FC curve in comparison to ZFC data is attributed to vortex pinning in type-II superconductor. Inset shows the enlarged view of the susceptibility data at low temperature. Fig. 5.4(b) depicts the isothermal field dependent magnetization of $SnTaS_2$ studied at 2 K. The magnetic hysteresis loop obtained suggests type-II superconductivity.

Further, to determine the lower critical magnetic field of $SnTaS_2$, the field dependence of magnetization at various temperature has been studied with a zero field cooling protocol. Inset of Fig. 5.5(a) shows isothermal magnetization at different

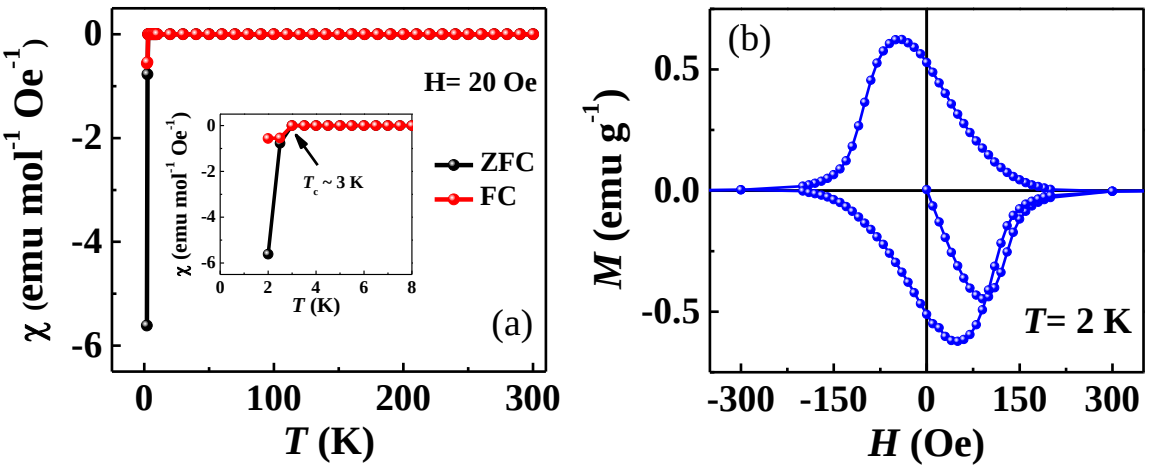

Figure 5.4. (a) Temperature dependent zero field cooled (ZFC) and field cooled (FC) magnetic susceptibility with an applied magnetic field of 20 Oe. Inset shows the extended data at low temperature region. (b) Isothermal field dependent magnetization studied at 2 K.

temperatures from 2 – 2.6 K and the solid green line is the linear fit to the low field data. As we increase the applied magnetic field the magnetization data starts to deviate from the linear fit giving a lower critical field H_{c1} for each isotherm. These lower critical field values are then fitted with the formula $H_{c1}(T) = H_{c1}(0)(1–t^2)$ where $t = T/T_c$ as shown by the solid red line in the main panel of Fig. 5.5(b). The zero temperature lower critical field is determined from the fit to be $\mu_0 H_{c1}(0) = 45.5$ Oe.

The Ginzburg-Landau superconducting penetration depth can be calculated from the formula $\mu_0 H_{c1}(0) = (\Phi_0/4\pi\lambda_{GL}^2) ln(\lambda_{GL}/\xi_{GL})$ and found to be approximately $\lambda_{GL}(0) = 243$ nm. Further, the Ginzburg-Landau parameter to be determined as $\kappa = \lambda_{GL}(0)/\xi_{GL}(0) = 5.12$ confirms that $SnTaS_2$ is a type-II superconductor. The thermodynamic critical field of $SnTaS_2$ can be determined from the relation $H_{c1}(0)H_{c2}(0) = H_c(0) ln(\kappa)$ and found to be $\mu_0 H_c(0) = 202$ Oe. The polycrystalline sample is having the coherence length and the penetration depth both in between of that for the $H||c$-direction and $H||ab$ plane of $SnTaS_2$ single crystal [44].

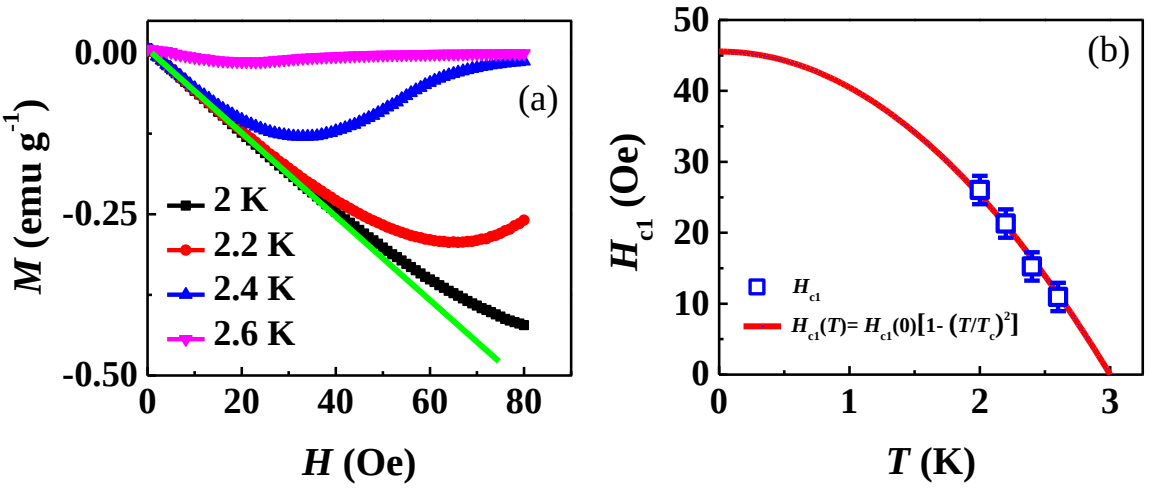

Figure 5.5. (a) Zero field cooled (ZFC) isothermal magnetization at different temperatures. The solid green line is the linear fit to the 2 K data in the low field range. (b) Lower critical field extracted from the isothermal magnetization curves. The solid red line represents the $H_{c1}(T) = H_{c1}(0)[1–(T/T_c)^2]$ fit to the temperature dependence of the lower critical fields.

5.4 Conclusions

Superconducting properties of polycrystalline $SnTaS_2$ have been studied in detail by means of structural, resistivity and magnetic measurements. $SnTaS_2$ crystallizes in a centrosymmetric hexagonal layered structure with $P6_3/mmc$ space group. $SnTaS_2$ is found to be superconducting below $T_c \sim 2.8$ K, with an upper critical field of $\mu_0 H_{c2}(0)$ = 1458 Oe and lower critical field of $\mu_0 H_{c1}(0) = 45.5$ Oe. The characteristic coherence length is found to be $\xi_{GL}(0) = 47.5$ nm, while the penetration depth is determined to be $\lambda_{GL}(0) = 243$ nm. The superconducting Ginzburg-Landau parameter $\kappa(0) = 5.12$ signifies $SnTaS_2$ to be a type-II superconductor.

Chapter 6

Summary and future outlook

The present chapter is an integration of the results discussed in the previous chapters. The thesis focussed on the design and development of new superconducting systems via the intercalation approach in layered transition metal dichalcogenides. A brief overview on the background of the field of superconductivity, following a vast literature survey has been presented in the first chapter of the thesis. The second chapter discusses the aspect of experimental procedures to synthesize and characterize the TMD based layered superconductors studied in this thesis. Physical properties, mainly the superconducting nature, of layered $PbNbS_2$, $PbNbSe_2$ and $SnTaS_2$ systems have been discussed in the next three chapters.

We report synthesis, crystal structure, electrical transport, magnetization and specific heat measurements to investigate the physical properties of $PbNbS_2$. Several key superconducting parameters have been determined to get insights of the nature of the superconductivity in this material. Superconductivity in layered moderately coupled $PbNbS_2$ system with a comparatively high T_c of 8.8 K offers a new avenue for several interesting studies.

Superconductivity and ferromagnetism are considered to be mutually exclusive electronic states which rarely found to coexist. We report concurrence of these two exotic phenomena in centrosymmetric $PbNbSe_2$. Superconductivity ($T_c \sim 5.75$ K) has been confirmed from the electrical resistivity and magnetic susceptibility

measurements. A weak ferromagnetism is observed to evolve in the close vicinity of superconductivity with ordering temperature $T_{FM} \sim 4.4$ K. Coexistence of superconductivity and ferromagnetism in layered $PbNbSe_2$ system offers a novel platform for exotic physics.

We also investigated the superconducting properties of polycrystalline $SnTaS_2$, synthesized by solid state reactions. Crystal structure, electrical transport and magnetic properties have been studied in detail. Key superconducting parameters have been determined to investigate the nature of superconductivity in this material. A comparative overview of superconductivity is given for the polycrystalline samples with the reported single crystal data.

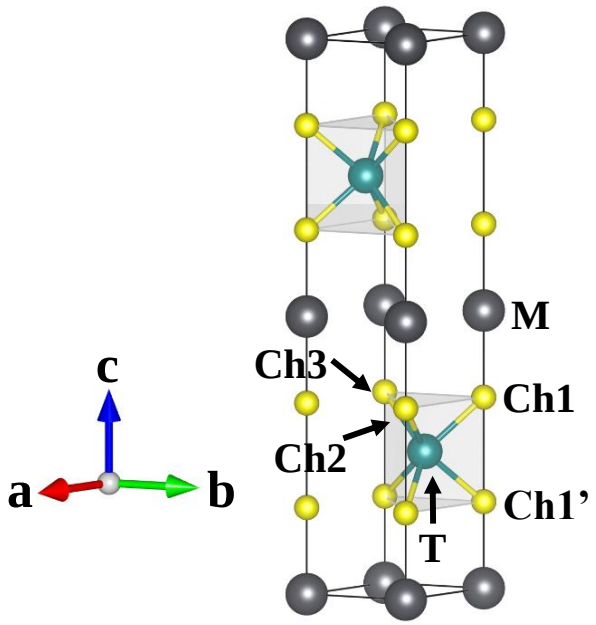

Figure 6.1. Crystal structure of generalized $MTCh_2$ system where M = Pb/Sn, T = Nb/Ta and Ch = S/Se. Ch1, Ch2, Ch3 and Ch1' belong to the same atomic site, and the nomenclature followed here is only for convention.

Table 6.1 represents the characteristic bond distances and bond angles of $PbNbS_2$, $PbNbSe_2$ and $SnTaS_2$ to give an insight of crystal structure of these systems.

Table 6.2 summerizes the characteristic superconducting parameters of $PbNbS_2$, $PbNbSe_2$ and $SnTaS_2$, and compares them with other related isoelectronic systems.

Table 6.1. Characteristic bond distances (Å) and bond angles (deg) of $PbNbS_2$, $PbNbSe_2$ and $SnTaS_2$ systems. Here M = Pb/Sn, T = Nb/Ta and Ch = S/Se (see Fig. 6.1).

Parameter	$PbNbS_2$	$PbNbSe_2$	$SnTaS_2$
Bond distances			
T − M	4.7979(10)	5.0374(3)	4.7500(3)
T − Ch1	2.5369(4)	2.8564(1)	2.2998(1)
M − Ch1	2.7421(7)	2.5747(1)	3.0635(2)
Ch1 − Ch2	3.3334(8)	3.4344(3)	3.3006(3)
Ch1 − Ch1'	3.3057(8)	4.1121(3)	2.5751(2)
Bond angles			
Ch1 − T − Ch2	82.141(14)	73.908(4)	91.711(4)
Ch1 − T − Ch1'	81.315(18)	92.077(5)	68.091(5)
Ch2 − T − Ch1'	135.418(7)	139.381(2)	131.050(1)
T − Ch1 − M	130.657(9)	136.038(3)	124.045(3)
Ref.	Chapter 3	Chapter 4	Chapter 5

Table 6.2. Superconducting parameters of $PbNbS_2$, $PbNbSe_2$, $SnTaS_2$ and related isoelectronic systems

Parameter	Unit	$PbTaSe_2$	$SnTaS_2$	$PbTaS_2$	$PbNbS_2$	$PbNbSe_2$	$SnTaS_2$
Sample		Polycrystalline	Single crystal	Single crystal	Polycrystalline	Polycrystalline	Polycrystalline
Space group		$P\bar{6}m2$	$P6_3/mmc$	$P6_3/mmc$	$P6_3/mmc$	$P6_3/mmc$	$P6_3/mmc$
T_c	K	3.72	3	2.6	8.8	5.75	2.8
$\mu_0 H_{c1}(0)$	mT	7.5	5.4[a],8.2[b]	3.4[a],4.1[b]	38.4		4.5
$\mu_0 H_{c2}(0)$	T	1.47	0.3[a],0.2[b]	0.3[a],0.5[b]	1.88	2.26	0.15
$\mu_0 H_P$	T	6.8	5.5	4.84	16.28	10.64	5.09
$\xi_{GL}(0)$	nm	15	127[a],8.5[b]	85.1[a],12.2[b]	13.2	12.1	47.5
$\lambda_{GL}(0)$	nm	248	64.4[a],962.4[b]	127.3[a],889.7[b]	90.94		243
$\kappa(0)$		17	7.6[a],5.1[b]	10.5[a],1.5[b]	6.89		5.12
$\gamma(0)$	mJ mol^{-1} K^{-2}	6.9	4.45	6.07	33.08		
$\Delta C/\gamma T_c$		1.41	1.23		1.54		
Θ_D	K	112	154.4	120	263.9		
λ_{ep}		0.74	0.66	0.69	0.81		
Ref.		[37]	[44]	[45]	Chapter 3	Chapter 4	Chapter 5

[a] : $H//ab$
[b] : $H//c$

The thesis introduces two new superconductors $PbNbS_2$ and $PbNbSe_2$ from the family of intercalated layered transition metal dichalcogenide systems. In addition, these systems are isoelectronic with related $PbTaSe_2$ [37, 40], $SnTaS_2$ [44] and $PbTaS_2$ [45], which are known to have nontrivial electronic structures that offers a promising platform to realize novel quantum states like topological superconductors and Majorana fermions. This makes $PbNbS_2$, $PbNbSe_2$ and ofcourse $SnTaS_2$ strong candidates for investigation of exotic topological properties, that may facilitate the future study of realizing 3D topological superconductors. This work opens a new

avenue to search for novel superconductors in related transition metal dichalcogenide syatems via intercalation approach.

Bibliography

[1] H. K. Onnes, Commun. Phys. Lab. Univ. Leiden. **120a, 122b, 124c** (1911).

[2] H. K. Onnes and W. H. Keesom, Commun. Phys. Lab. Univ. Leiden. **133d** (1913).

[3] V. L. Ginzburg and D. A. Kirzhnits, Nauka, Moscow, 1977.

[4] W. Meissner and R. Ochsenfeld, Naturwissenschaften **21**, 787 (1933).

[5] F. London and H. London, Proc. Roy. Soc. (London) **A149**, 71 (1935).

[6] V. L. Ginzburg and L. D. Landau, Zh. Eksperim. i Teor. Fiz. **20**, 1064 (1950).

[7] V. L. Ginzburg and L. D. Landau, *On the Theory of Superconductivity*, pp. 113–137, Springer Berlin Heidelberg, Berlin, Heidelberg, 2009.

[8] H. Fröhlich, Phys. Rev. **79**, 845 (1950).

[9] E. Maxwell, Phys. Rev. **78**, 477 (1950).

[10] C. A. Reynolds, B. Serin, W. H. Wright, and L. B. Nesbitt, Phys. Rev. **78**, 487 (1950).

[11] J. Bardeen, L. N. Cooper, and J. R. Schrieffer, Phys. Rev. **108**, 1175 (1957).

[12] J. Bednorz and K. Müller, Z. Phys. B **64**, 189 (1986).

[13] M. K. Wu, J. R. Ashburn, C. J. Torng, P. H. Hor, R. L. Meng, L. Gao, Z. J. Huang, Y. Q. Wang, and C. W. Chu, Phys. Rev. Lett. **58**, 908 (1987).

[14] J. L. Tallon, R. G. Buckley, P. W. Gilberd, M. R. Presland, I. W. M. Brown, M. E. Bowden, L. A. Christian, and R. Goguel, Nature **333**, 153 (1988).

[15] Z. Sheng and A. Hermann, Nature **332**, 138 (1988).

[16] A. Schilling, M. Cantoni, J. D. Guo, and H. R. Ott, Nature **363**, 56 (1993).

[17] Y. Kamihara, H. Hiramatsu, M. Hirano, R. Kawamura, H. Yanagi, T. Kamiya, and H. Hosono, J. Am. Chem. Soc. **128**, 10012 (2006).

[18] Y. Kamihara, T. Watanabe, M. Hirano, and H. Hosono, J. Am. Chem. Soc. **130**, 3296 (2008).

[19] S. Matsuishi, Y. Inoue, T. Nomura, H. Yanagi, M. Hirano, and H. Hosono, J. Am. Chem. Soc. **130**, 14428 (2008).

[20] M. Rotter, M. Tegel, and D. Johrendt, Phys. Rev. Lett. **101**, 107006 (2008).

[21] F.-C. Hsu, J.-Y. Luo, K.-W. Yeh, T.-K. Chen, T.-W. Huang, P. M. Wu, Y.-C. Lee, Y.-L. Huang, Y.-Y. Chu, D.-C. Yan, and M.-K. Wu, Proc. Natl. Acad. Sci. **105**, 14262 (2008).

[22] X. Wang, Q. Liu, Y. Lv, W. Gao, L. Yang, R. Yu, F. Li, and C. Jin, Solid State Commun. **148**, 538 (2008).

[23] J. Guo, S. Jin, G. Wang, S. Wang, K. Zhu, T. Zhou, M. He, and X. Chen, Phys. Rev. B **82**, 180520 (2010).

[24] A. Iyo, K. Kawashima, T. Kinjo, T. Nishio, S. Ishida, H. Fujihisa, Y. Gotoh, K. Kihou, H. Eisaki, and Y. Yoshida, J. Am. Chem. Soc. **138**, 3410 (2016).

[25] Z.-C. Wang, C.-Y. He, S.-Q. Wu, Z.-T. Tang, Y. Liu, A. Ablimit, C.-M. Feng, and G.-H. Cao, J. Am. Chem. Soc. **138**, 7856 (2016).

[26] Z.-C. Wang, C.-Y. He, S.-Q. Wu, Z.-T. Tang, Y. Liu, and G.-H. Cao, Chem. Mater. **29**, 1805 (2017).

[27] M. Fujioka, S. J. Denholme, T. Ozaki, H. Okazaki, K. Deguchi, S. Demura, H. Hara, T. Watanabe, H. Takeya, T. Yamaguchi, H. Kumakura, and Y. Takano, Supercond. Sci. Technol. **26**, 085023 (2013).

[28] Y. Mizuguchi, H. Fujihisa, Y. Gotoh, K. Suzuki, H. Usui, K. Kuroki, S. Demura, Y. Takano, H. Izawa, and O. Miura, Phys. Rev. B **86**, 220510 (2012).

[29] Y. Mizuguchi, S. Demura, K. Deguchi, Y. Takano, H. Fujihisa, Y. Gotoh, H. Izawa, and O. Miura, J. Phys. Soc. Jpn. **81**, 114725 (2012).

[30] M. Nagao, S. Demura, K. Deguchi, A. Miura, S. Watauchi, T. Takei, Y. Takano, N. Kumada, and I. Tanaka, J. Phys. Soc. Jpn. **82**, 113701 (2013).

[31] X. Lin, X. Ni, B. Chen, X. Xu, X. Yang, J. Dai, Y. Li, X. Yang, Y. Luo, Q. Tao, G. Cao, and Z. Xu, Phys. Rev. B **87**, 020504 (2013).

[32] D. Yazici, K. Huang, B. D. White, I. Jeon, V. W. Burnett, A. J. Friedman, I. K. Lum, M. Nallaiyan, S. Spagna, and M. B. Maple, Phys. Rev. B **87**, 174512 (2013).

[33] H.-F. Zhai, P. Zhang, S.-Q. Wu, C.-Y. He, Z.-T. Tang, H. Jiang, Y.-L. Sun, J.-K. Bao, I. Nowik, I. Felner, Y.-W. Zeng, Y.-K. Li, X.-F. Xu, Q. Tao, Z.-A. Xu, and G.-H. Cao, J. Am. Chem. Soc. **136**, 15386 (2014).

[34] E. Revolinsky, E. P. Lautenschlager, and C. H. Armitage, Solid State Commun. **1**, 59 (1963).

[35] F. Jellinek, G. Brauer, and H. Müller, Nature **185**, 376 (1960).

[36] S. Nagata, T. Aochi, T. Abe, S. Ebisu, T. Hagino, Y. Seki, and K. Tsutsumi, J. Phys. Chm. Solids **53**, 1259 (1992).

[37] M. N. Ali, Q. D. Gibson, T. Klimczuk, and R. J. Cava, Phys. Rev. B **89**, 020505 (2014).

[38] C.-L. Zhang, Z. Yuan, G. Bian, S.-Y. Xu, X. Zhang, M. Z. Hasan, and S. Jia, Phys. Rev. B **93**, 054520 (2016).

[39] G. M. Pang, M. Smidman, L. X. Zhao, Y. F. Wang, Z. F. Weng, L. Q. Che, Y. Chen, X. Lu, G. F. Chen, and H. Q. Yuan, Phys. Rev. B **93**, 060506 (2016).

[40] G. Bian, T.-R. Chang, R. Sankar, S.-Y. Xu, H. Zheng, T. Neupert, C.-K. Chiu, S.-M. Huang, G. Chang, I. Belopolski, D. S. Sanchez, M. Neupane, N. Alidoust, C. Liu, B. Wang, C.-C. Lee, H.-T. Jeng, C. Zhang, Z. Yuan, S. Jia, A. Bansil, F. Chou, H. Lin, and M. Z. Hasan, Nat. Commun. **7**, 10556 (2016).

[41] S.-Y. Guan, P.-J. Chen, M.-W. Chu, R. Sankar, F. Chou, H.-T. Jeng, C.-S. Chang, and T.-M. Chuang, Sci. Adv. **2**, e1600894 (2016).

[42] U. S. Kaluarachchi, Y. Deng, M. F. Besser, K. Sun, L. Zhou, M. C. Nguyen, Z. Yuan, C. Zhang, J. S. Schilling, M. J. Kramer, S. Jia, C.-Z. Wang, K.-M. Ho, P. C. Canfield, and S. L. Bud'ko, Phys. Rev. B **95**, 224508 (2017).

[43] C. Q. Xu, R. Sankar, W. Zhou, B. Li, Z. D. Han, B. Qian, J. H. Dai, H. Cui, A. F. Bangura, F. C. Chou, and X. Xu, Phys. Rev. B **96**, 064528 (2017).

[44] D.-Y. Chen, Y. Wu, L. Jin, Y. Li, X. Wang, J. Duan, J. Han, X. Li, Y.-Z. Long, X. Zhang, D. Chen, and B. Teng, Phys. Rev. B **100**, 064516 (2019).

[45] J. J. Gao, J. G. Si, X. Luo, J. Yan, Z. Z. Jiang, W. Wang, C. Q. Xu, X. F. Xu, P. Tong, W. H. Song, X. B. Zhu, W. J. Lu, and Y. P. Sun, J. Phys. Chem. C **124**, 6349 (2020).

[46] J. Nagamatsu, N. Nakagawa, T. Muranaka, Y. Zenitani, and J. Akimitsu, Nature **410**, 63 (2001).

[47] R. Nagarajan, C. Mazumdar, Z. Hossain, S. K. Dhar, K. V. Gopalakrishnan, L. C. Gupta, C. Godart, B. D. Padalia, and R. Vijayaraghavan, Phys. Rev. Lett. **72**, 274 (1994).

[48] R. J. Cava, H. Takagi, H. W. Zandbergen, J. J. Krajewski, W. F. Peck, T. Siegrist, B. Batlogg, R. B. van Dover, R. J. Felder, K. Mizuhashi, J. O. Lee, H. Eisaki, and S. Uchida, Nature **367**, 252 (1994).

[49] E. Bauer, G. Hilscher, H. Michor, C. Paul, E. W. Scheidt, A. Gribanov, Y. Seropegin, H. Noël, M. Sigrist, and P. Rogl, Phys. Rev. Lett. **92**, 027003 (2004).

[50] A. P. Drozdov, M. I. Eremets, I. A. Troyan, V. Ksenofontov, and S. I. Shylin, Nature **525**, 73 (2015).

[51] A. P. Drozdov, P. P. Kong, V. S. Minkov, S. P. Besedin, M. A. Kuzovnikov, S. Mozaffari, L. Balicas, F. F. Balakirev, D. E. Graf, V. B. Prakapenka, E. Greenberg, D. A. Knyazev, M. Tkacz, and M. I. Eremets, Nature **569**, 528 (2019).

[52] C. Heil, S. di Cataldo, G. B. Bachelet, and L. Boeri, Phys. Rev. B **99**, 220502 (2019).

[53] E. Snider, N. Dasenbrock-Gammon, R. McBride, M. Debessai, H. Vindana, K. Vencatasamy, K. V. Lawler, A. Salamat, and R. P. Dias, Nature **586**, 373 (2020).

[54] N. R. Werthamer, E. Helfand, and P. C. Hohenberg, Phys. Rev. **147**, 295 (1966).

[55] A. M. Clogston, Phys. Rev. Lett. **9**, 266 (1962).

[56] B. S. Chandrasekhar, Appl. Phys. Lett. **1**, 7 (1962).

[57] R. E. Peierls, Oxford University Press, 1955.

[58] R. E. Peierls, Princeton University Press, 1991.

[59] H. Fröhlich, Proc. R. Soc. A **223**, 296 (1954).

[60] K. Rossnagel, J. Phys.: Condens. Matter **23**, 213001 (2011).

[61] J. A. Wilson, F. J. Di Salvo, and S. Mahajan, Adv Phys. **50**, 1171 (2001).

[62] F. Soto, H. Berger, L. Cabo, C. Carballeira, J. Mosqueira, D. Pavuna, P. Toimil, and F. Vidal, Physica C: Superconductivity **460-462**, 789 (2007).

[63] D. Lin, S. Li, J. Wen, H. Berger, L. Forró, H. Zhou, S. Jia, T. Taniguchi, K. Watanabe, X. Xi, and M. S. Bahramy, Nat Commun **11**, 2406 (2020).

[64] B. E. Brown and D. J. Beerntsen, Acta Cryst. **18**, 31 (1965).

[65] G. C. Trigunayat and A. R. Verma, *Polytypism and Stacking Faults in Crystals with Layer Structure*, pp. 269–340, Springer Netherlands, Dordrecht, 1976.

[66] A. Thompson, R. Gamble, and J. Revelli, Solid State Commun. **9**, 981 (1971).

[67] B. Sipos, A. F. Kusmartseva, A. Akrap, H. Berger, L. Forró, and A. Tutiš, Nat. Mat. **7**, 960 (2008).

[68] S. ichi Nohara, H. Namatame, H. Matsubara, M. Fujisawa, M. Naitou, S. Tanaka, H. Negishi, M. Inoue, H. Sakamoto, A. Misu, and S. Suga, J. Phys. Soc. Jpn **60**, 3882 (1991).

[69] U. Dutta, P. S. Malavi, S. Sahoo, B. Joseph, and S. Karmakar, Phys. Rev. B **97**, 060503 (2018).

[70] S. Sahoo, U. Dutta, L. Harnagea, A. K. Sood, and S. Karmakar, Phys. Rev. B **101**, 014514 (2020).

[71] X.-C. Pan, X. Chen, H. Liu, Y. Feng, Z. Wei, Y. Zhou, Z. Chi, L. Pi, F. Yen, F. Song, X. Wan, Z. Yang, B. Wang, G. Wang, and Y. Zhang, Nat. Commun. **6**, 7805 (2015).

[72] Y. Qi, P. G. Naumov, M. N. Ali, C. R. Rajamathi, W. Schnelle, O. Barkalov, M. Hanfland, S.-C. Wu, C. Shekhar, Y. Sun, V. Süβ, M. Schmidt, U. Schwarz,

E. Pippel, P. Werner, R. Hillebrand, T. Förster, E. Kampert, S. Parkin, R. J. Cava, C. Felser, B. Yan, and S. A. Medvedev, Nat. Commun. **7**, 11038 (2016).

[73] J. P. Tidman, O. Singh, A. E. Curzon, and R. F. Frindt, Phil. Mag. **30**, 1191 (1974).

[74] K. Tsutsumi, Y. Ishihara, and H. Suzuki, Solid State Commun. **74**, 1099 (1990).

[75] P. Garoche, P. Manuel, and J. Veyssié, J. Low Temp. Phys. **30**, 323 (1978).

[76] J. Wilson, F. D. Salvo, and S. Mahajan, Adv. Phys. **24**, 117 (1975).

[77] R. Liu, W. C. Tonjes, V. A. Greanya, C. G. Olson, and R. F. Frindt, Phys. Rev. B **61**, 5212 (2000).

[78] D. S. Inosov, V. B. Zabolotnyy, D. V. Evtushinsky, A. A. Kordyuk, B. Büchner, R. Follath, H. Berger, and S. V. Borisenko, New J. Phys. **10**, 125027 (2008).

[79] K. Onabe, M. Naito, and S. Tanaka, J. Phys. Soc. Jpn. **45**, 50 (1978).

[80] M. Naito and S. Tanaka, J. Phys. Soc. Jpn. **51**, 219 (1982).

[81] P. Moliniè, D. Jérome, and A. J. Grant, Phil. Mag. **30**, 1091 (1974).

[82] B. W. Pfalzgraf and H. Spreckels, J. Phys. C **20**, 4359 (1987).

[83] Y. Hamaue and R. Aoki, J. Phys. Soc. Jpn. **55**, 1327 (1986).

[84] I. Guillamón, H. Suderow, S. Vieira, L. Cario, P. Diener, and P. Rodière, Phys. Rev. Lett. **101**, 166407 (2008).

[85] V. G. Tissen, M. R. Osorio, J. P. Brison, N. M. Nemes, M. García-Hernández, L. Cario, P. Rodière, S. Vieira, and H. Suderow, Phys. Rev. B **87**, 134502 (2013).

[86] H. Hess, Physica C **185-189**, 259 (1991).

[87] H. F. Hess, R. B. Robinson, and J. V. Waszczak, Phys. Rev. Lett. **64**, 2711 (1990).

[88] R. A. Klemm, *Layered Superconductors*, volume 1, Oxford University Press, 2012.

[89] W. C. Tonjes, V. A. Greanya, R. Liu, C. G. Olson, and P. Molinié, Phys. Rev. B **63**, 235101 (2001).

[90] E. Revolinsky, G. Spiering, and D. Beerntsen, J. Phys. Chem. Solids **26**, 1029 (1965).

[91] P. Garoche, J. Veyssié, P. Manuel, and P. Molinié, Solid State Commun. **19**, 455 (1976).

[92] C. Oglesby, E. Bucher, C. Kloc, and H. Hohl, J. Cryst. Growth **137**, 289 (1994).

[93] U. Yaron, P. L. Gammel, D. A. Huse, R. N. Kleiman, C. S. Oglesby, E. Bucher, B. Batlogg, D. J. Bishop, K. Mortensen, K. Clausen, C. A. Bolle, and F. De La Cruz, Phys. Rev. Lett. **73**, 2748 (1994).

[94] P. Koorevaar, J. Aarts, P. Berghuis, and P. H. Kes, Phys. Rev. B **42**, 1004 (1990).

[95] R. F. Frindt, Phys. Rev. Lett. **28**, 299 (1972).

[96] S. Foner and E. McNiff, Phys. Lett. A **45**, 429 (1973).

[97] P. de Trey, S. Gygax, and J. P. Jan, J. Low Temp. Phys. **11**, 421 (1973).

[98] D. Jérome, A. Grant, and A. Yoffe, Solid State Commun. **9**, 2183 (1971).

[99] D. Sanchez, A. Junod, J. Muller, H. Berger, and F. Lévy, Physica B **204**, 167 (1995).

[100] R. E. Jones, H. R. Shanks, D. K. Finnemore, and B. Morosin, Phys. Rev. B **6**, 835 (1972).

[101] A. J. Bevolo and H. R. Shanks, J. Appl. Phys. **45**, 4644 (1974).

[102] C. W. Chu, V. Diatschenko, C. Y. Huang, and F. J. DiSalvo, Phys. Rev. B **15**, 1340 (1977).

[103] H. N. S. Lee, H. McKinzie, D. S. Tannhauser, and A. Wold, J. Appl. Phys. **40**, 602 (1969).

[104] J. Edwards and R. Frindt, J. Phys. Chem. Solids **32**, 2217 (1971).

[105] R. C. Morris, R. V. Coleman, and R. Bhandari, Phys. Rev. B **5**, 895 (1972).

[106] L. F. Mattheiss, Phys. Rev. B **8**, 3719 (1973).

[107] H. F. Hess, R. B. Robinson, R. C. Dynes, J. M. Valles, and J. V. Waszczak, Phys. Rev. Lett. **62**, 214 (1989).

[108] D. A. Whitney, R. M. Fleming, and R. V. Coleman, Phys. Rev. B **15**, 3405 (1977).

[109] A. A. Abrikosov and L. P. Gor'kov, Zh. Eksp. Teor. Fiz. **39**, 1781 (1960), [Sov. Phys. JETP 12, 1243 (1961)].

[110] K. E. Wagner, E. Morosan, Y. S. Hor, J. Tao, Y. Zhu, T. Sanders, T. M. McQueen, H. W. Zandbergen, A. J. Williams, D. V. West, and R. J. Cava, Phys. Rev. B **78**, 104520 (2008).

[111] F. J. Di Salvo, G. W. Hull, L. H. Schwartz, J. M. Voorhoeve, and J. V. Waszczak, J. Chem. Phys. **59**, 1922 (1973).

[112] J. Dijkstra, E. A. Broekhuizen, C. F. van Bruggen, C. Haas, R. A. de Groot, and H. P. van der Meulen, Phys. Rev. B **40**, 12111 (1989).

[113] F. Lévy (ed.), *Intercalated Layered Materials*, volume 1, Springer Netherlands, 1979.

[114] R. B. Somoano and A. Rembaum, Phys. Rev. Lett. **27**, 402 (1971).

[115] J. A. Woollam, R. B. Somoano, and P. O'Connor, Phys. Rev. Lett. **32**, 712 (1974).

[116] L. Fang, Y. Wang, P. Y. Zou, L. Tang, Z. Xu, H. Chen, C. Dong, L. Shan, and H. H. Wen, Phys. Rev. B **72**, 014534 (2005).

[117] N. Ahmad, P. C. Klipstein, S. D. Obertelli, E. A. Marseglia, and R. H. Friend, J. Phys. C: Solid State Phys. **20**, 4105 (1987).

[118] Y. Ōnuki, S. Yamanaka, R. Inada, M. Kido, and S. Tanuma, Synth. Met. **5**, 245 (1983).

[119] J. T. Ye, Y. J. Zhang, R. Akashi, M. S. Bahramy, R. Arita, and Y. Iwasa, Science **338**, 1193 (2012).

[120] E. Morosan, H. W. Zandbergen, B. S. Dennis, J. W. G. Bos, Y. Onose, T. Klimczuk, A. P. Ramirez, N. P. Ong, and R. J. Cava, Nat. Phys. **2**, 544 (2006).

[121] P.-J. Chen, T.-R. Chang, and H.-T. Jeng, Phys. Rev. B **94**, 165148 (2016).

[122] B.-T. Wang, P.-F. Liu, J.-J. Zheng, W. Yin, and F. Wang, Phys. Rev. B **98**, 014514 (2018).

[123] A. R. West, Wiley, 1984.

[124] Bruker AXS, Germany, Topas 4.2, 2009.

[125] R. Micnas, J. Ranninger, and S. Robaszkiewicz, Rev. Mod. Phys. **62**, 113 (1990).

[126] A. B. Karki, Y. M. Xiong, N. Haldolaarachchige, S. Stadler, I. Vekhter, P. W. Adams, D. P. Young, W. A. Phelan, and J. Y. Chan, Phys. Rev. B **83**, 144525 (2011).

[127] M. D. Lan, J. C. Chang, K. T. Lu, C. Y. Lee, H. Y. Shih, and G. Y. Jeng, IEEE Trans. Appl. Supercond. **11**, 3607 (2001).

[128] K. Maki, Phys. Rev. **148**, 362 (1966).

[129] P. Fulde and R. A. Ferrell, Phys. Rev. **135**, A550 (1964).

[130] A. I. Larkin and Y. N. Ovchinnikov, Zh. Eksp. Teor. Fiz. **47**, 1136 (1964), [Sov. Phys. JETP 20, 762 (1965)].

[131] W. L. McMillan, Phys. Rev. **167**, 331 (1968).

[132] Z. Ren, Q. Tao, S. Jiang, C. Feng, C. Wang, J. Dai, G. Cao, and Z. Xu, Phys. Rev. Lett. **102**, 137002 (2009).

[133] S. Nandi, W. T. Jin, Y. Xiao, Y. Su, S. Price, D. K. Shukla, J. Strempfer, H. S. Jeevan, P. Gegenwart, and T. Brückel, Phys. Rev. B **89**, 014512 (2014).

[134] U. Pachmayr, F. Nitsche, H. Luetkens, S. Kamusella, F. Brückner, R. Sarkar, H.-H. Klauss, and D. Johrendt, Angew. Chem. Int. Ed. **53**, 1 (2014).

[135] A. Tsvyashchenko, V. Sidorov, A. Petrova, L. Fomicheva, I. Zibrov, and V. Dmitrienko, J. Alloys Compd. **686**, 431 (2016).

[136] X. Zhu, Y. Guo, H. Cheng, J. Dai, X. An, J. Zhao, K. Tian, S. Wei, X. Cheng Zeng, C. Wu, and Y. Xie, Nat. Commun. **7**, 11210 (2016).

Vita

Soumen Ash joined the Institute of Nano Science and Technology Mohali (INST Mohali) in August 2014 for his doctoral dissertation by research, and registered at the Indian Institute of Science Education and Research Mohali (IISER Mohali) for the award of the degree of Doctor of Philosophy. He has earned his Bachelor of Science degree in Physics (honours) from the University of Calcutta, Kolkata and Master of Science degree in Applied Physics from Indian School of Mines, Dhanbad (currently Indian Institute of Technology (ISM) Dhanbad). He has qualified the all India basis Graduate Aptitude Test in Engineering 2013 (GATE-2013) in Physics. He also qualified the all India basis Joint CSIR-UGC Test for Junior Research Fellowship and Eligibility for Lectureship (NET-JRF) in 2017. He is the recipient of the best poster award in the National Conference on Advanced Functional Materials 2019 (NCFM-2019). He has carried out his doctoral research work under the joint supervision of Prof. Ashok K. Ganguli (IIT Delhi) and Prof. Hirendra N. Ghosh (INST Mohali). His scientific expertise and area of research include solid state synthesis of intermetallic compounds and to study their crystal structure and physical properties, mainly focussed on superconductivity and magnetism.

Soumen Ash